J. Fluid Mech. (2003), *vol.* 488, *pp.* 151–188.
DOI: 10.1017/S0022112003004804 Printed in the United Kingdom

Wall-transpiration-induced instabilities in plane Couette flow

By J. M. FLORYAN

Department of Mechanical and Materials Engineering, The University of Western Ontario, London, Ontario, N6A 5B9, Canada

(Received 8 April 2002 and in revised form 7 March 2003)

Linear stability of Couette flow modified by transpiration applied at the lower wall is considered. It is shown that transpiration can induce flow instability resulting in the appearance of streamwise-vortex-like structures. It is argued that the instability is driven by centrifugal forces associated with streamline curvature. The conditions leading to the onset of the instability depend on the amplitude and wavelength of the transpiration and can be expressed in terms of the critical Reynolds number. The global critical conditions describing the minimum critical Reynolds number required for the onset of the instability for the specified amplitude of the transpiration regardless of its wavelength are also given. The threshold amplitude required for the onset varies approximately as $\sim Re^{-1.15}$ for large Re, where the Reynolds number used is based on the velocity difference between the walls and the channel half-width. The existence of a global threshold, below which the instability cannot occur regardless of the amplitude of the transpiration, has been demonstrated. This threshold corresponds approximately to $Re = 84$.

1. Introduction

These has been remarkable progress in recent years in understanding of transition to turbulence. This is especially true for systems undergoing supercritical primary bifurcations. Supercriticality is characterized by the existence of a bifurcated state above a certain linear stability threshold expressed in terms of a critical Reynolds number Re_{cr}. Above the threshold, the system is unstable to infinitesimal disturbances but remains closed to the basic state, yielding a continuous transition as Re increases. Its evolution can be followed for small distance above Re_{cr} using weakly nonlinear stability theory. Rayleigh–Bénard convection is a good prototype of such a system. In contrast, in the subcritical case the bifurcated state co-exists with the basic state below the threshold. Since the bifurcated state is at a finite distance from the basic state, the transition is discontinuous. Plane Poiseuille flow provides a good example of such a system. The case of plane Couette flow is more dramatic as it never becomes linearly unstable (Romanov 1973). It has been observed, nevertheless, that this flow undergoes transition at Reynolds numbers (based on the velocity difference between the walls and the channel half-width) as low as between 600 and 800 (Tillmark & Alfredsson 1992; Daviaud, Hegseth & Bergé 1992). This makes Couette flow particularly attractive for the study of non-trivial nonlinear states as well as for the study of the so-called bypass transition. The term 'by-pass transition' loosely denotes any scenario that does not rely on the growth of the least stable eigenmode.

The transition process in Couette flow may be 'natural', where the threshold depends on the noise level, or could be 'triggered' by introduction of special disturbances. The experimental data are very limited, mainly due to the difficulties in creating a well-controlled flow. Leutheusser & Chu (1971) and Aydin & Leutheusser (1979) considered 'natural transition' and gave the threshold at $Re \approx 600$ while Malerud, Måløy & Goldburg (1995) estimated it to be $Re \approx 740$. Tillmark & Alfredson (1992) showed that isolated, localized, instantaneous pulses could destabilize the flow for $Re \approx 720$. Daviaud *et al.* (1992) used a slightly different configuration and obtained $Re \approx 740$. Direct numerical simulations (Lundbladh & Johansson 1991) showed the existence of sustained turbulent spots for $Re > 750$. Dauchot & Daviaud (1995*a*) suggested the existence of a critical disturbance amplitude, which is a function of Re. This amplitude decreases rapidly when Re is reduced to $Re \approx 650$. Experiments by Bottin *et al.* (1998*b*) and Bottin & Chaté (1998), involving quenching the flow down from sufficiently large Reynolds numbers, confirmed $Re \approx 650$ to be the lower stability limit for turbulent flow. This is in agreement with the numerical experiments of Hamilton, Kim & Waleffe (1995), that demonstrated that turbulent Couette flow could not be maintained below $Re \approx 660$.

One approach in the theoretical analysis of transition in Couette flow is to assume that 'bifurcation' occurs at $Re = \infty$ and to seek finite-amplitude solutions at a finite Reynolds number (preferably corresponding to the experimentally observed values). As the number and configuration of fixed points of the relevant dynamical system is unknown, the approach followed involves continuation from an 'adjacent' known non-trivial fixed point. Nagata (1990) considered Taylor–Couette flow and in the limit of zero rotation isolated steady solutions in the form of modulated rolls oriented along the flow. These rolls exist down to $Re \approx 250$. Clever & Busse (1992, 1997) found the same solutions in the case of the Bénard–Couette problem of fluid heated from below in the limit of vanishing Rayleigh number. Barkley & Tuckerman (1999) carried out a stability analysis of Couette flow modified by a spanwise ribbon and found a subcritical instability giving rise to streamwise vortices with a critical value of Re about 460. They did not determine saturation states. Cherhabili & Ehrenstein (1995) found a different class of solutions by extending nonlinear equilibrium states for two-dimensional travelling waves from Poiseuille–Couette flow to Couette limit. Such states, which become stationary in the limit, may exist only for $Re \geqslant 3000$. They may evolve into new three-dimensional states that can exist for $Re \geqslant 2000$ (Cherhabili & Ehrenstein 1997). These structures are possibly less relevant to transition as they occur at Re much higher than the observed transitional Reynolds number. Longitudinal rolls are important as they represent key ingredients of the cyclic process possibly responsible for transition (Hamilton *et al.* 1995; Waleffe 1997; Reddy *et al.* 1998); this process involves streamwise vortices turning into streaks, breakdown of streaks into turbulence, and subsequent regeneration of vortices after damping of small-scale motions. There is, however, little direct experimental evidence for their existence. Dauchot & Daviaud (1995*b*) demonstrated the existence of streamwise vortices in Couette flow modified by a spanwise wire. Bottin, Dauchot & Daviaud (1998*a*) discussed experiments with turbulent spots as well as spanwise wires which indirectly support conjecture that a related non-trivial solution exists. Stability analysis of modified Couette flow (Barkley & Tuckerman 1999) showed that vortices originate from subcritical instability and thus supports such conjecture.

An alternative approach is to look directly at the initial value problems. In the case of linearized systems, all disturbances must eventually decay, with the slowest decaying

mode being spanwise invariant due to Squire's theorem. The existence of a slowly decaying mode may give rise to a three-dimensional, exponentially growing instability (Orszag & Patera 1983). This instability does not occur for Re less than about 2000 and requires finite magnitude of the primary mode. A large temporal growth of infinitesimal disturbances is possible due to the non-normality of the operator. This growth could be $O(1000)$ in the case of initial conditions corresponding to streamwise vortices for transitional Re (Butler & Farrell 1992); it increases proportionally to Re^2 for large Re (Schmid & Henningson 2001) and can trigger nonlinear effects (Trefethen *et al.* 1993). There is a related question of the threshold value for the initial size of disturbances. Perturbations decay to zero below this threshold and may lead to turbulence above this threshold. It has been suggested that the threshold decreases as $Re^{-\gamma}$ (Trefethen *et al.* 1993). Calculations by Reddy *et al.* (1998) suggest a γ-value of approximately 5/4. Asymptotic analysis by Chapman (2002) suggests an approximate γ-value of 1. Kreiss, Lundbladh & Henningson (1994) showed the upper limit of γ to be 21/4.

The third approach considers effects of slight perturbations in Couette flow on the stability characteristics with the premise that the experimentally observed Couette flow is never ideal. Trefethen *et al.* (1993) demonstrated extreme sensitivity of spectra of non-normal operators to perturbations of the operator, suggesting that slightly perturbed Couette flow may be linearly unstable. Lerner & Knobloch (1988) considered a small defect in Couette flow and demonstrated that it leads to an inviscid linear instability. Dubrulle & Zahn (1991) generalized this approach by adding viscous effects. Dauchot & Daviaud (1995*b*) disturbed the flow by placing a wire in the spanwise direction and observed instability in the form of streamwise vortices. Theoretical analysis of the flow modified in a similar manner showed subcritical instability (Barkley & Tuckerman 1999). Floryan (2002) considered Couette flow over a wavy wall and demonstrated the existence of instability driven by a centrifugal effect. Bottaro, Corbett & Luchini (2003) identified the form of the base-flow variations that has the largest effect on the eigenvalues.

The presence of spatially varying wall transpiration deflects particles from otherwise rectilinear trajectories. The resulting streamlines are curved, giving rise to a centrifugal force field that can potentially activate the inviscid instability mechanism first discussed by Rayleigh (1916). The characteristic signature of this instability is that the amplified disturbances have the form of counter-rotating vortices with axis parallel to the flow direction. Taylor (1923) demonstrated the existence of this instability in viscous flow between concentric rotating cylinders. Dean (1928) analysed similar instability in curved channels. Görtler (1941) demonstrated its existence in boundary layers over concave surfaces. Floryan (1986) showed that the instability is active in flows over concave as well as convex surfaces. The wall curvature was constant in all these studies, permitting description of the critical stability conditions in terms of a single parameter.

The general objective of this paper is to investigate the effect of variable transpiration (suction/blowing) applied at the lower wall. Transpiration represents a non-intrusive method for flow control and thus it is interesting to identify its optimal properties, i.e. the form of the 'smallest' transpiration that produces the 'largest' changes in the flow. Loudspeakers connected to perforated wall segments can produce transpiration with zero mean, providing a wide range of options for flow forcing. In this sense, wall transpiration is similar to synthetic jets, which are being widely studied at present (Glezer & Amitay 2002). Loudspeakers have been used widely as a source of controlled external disturbances in the analysis of laminar–turbulent transition in

boundary layers (Saric, Reed & Kerschen 2002; Saric, Reed & White 2003), but not as a controlling agent.

It is plausible that a large enough transpiration may lead to a major re-alignment of the flow. Since large transpiration implies large cost, it is interesting to identify the smallest possible transpiration that is able to transform the flow in a permanent manner, i.e. it is capable of pushing the flow through a stability limit. This goal can be achieved by focusing the search on the spatial distributions rather than on the amplitudes of the transpiration. Such a strategy is likely to succeed as weak transpiration represents a tool for creation of perturbations in Couette flow; this flow is very sensitive to the presence of perturbations as discussed above. Apart from the flow control applications, the effects of transpiration are of interest from the fundamental point of view in the area of analysis of variations of spectra as a function of mean flow perturbations.

Since ideal Couette flow is linearly stable (Romanov 1972), there are no guidelines regarding values of Re that could offer opportunities for generation of instabilities on the linear level. This investigation considers therefore a wide range of Re, from $Re = O(1)$ to $Re = O(10^5)$. In order to make the analysis tractable, attention is focused on disturbances in the form of streamwise vortices only. The potential appearance of travelling wave instability is not considered.

The appearance of streamwise vortices in flows with streamwise periodic modulation has been identified on a number of occasions. In the case of Langmuir circulation, the spatial modulation is created by a wavy interface via Stokes drift (Craik 1982; Leibovich 1977). The resulting vortices are attributed to the action of a centrifugal effect and the corresponding mechanism is referred to as the CL2 mechanism (Leibovich 1983). The CL1 mechanism, related to bending of the vortex sheets (Craik & Lebovich 1976), can be a contributing factor. The second example involves spatial modulation induced by a wavy wall. Tokuda (1972) postulated that this flow might be subject to the centrifugal-force-driven instability, giving rise to streamwise vortices. Similar vortices can be created by the CL2 mechanism, which can also operate in a non-centrifugal regime (Phillips & Wu 1994; Phillips, Wu & Lumley 1996). The necessary conditions for the latter instability are expressed in terms of the Craik–Phillips–Shen criterion (Phillips 1998). Saric & Benmalik (1991) analysed boundary layers over a wavy surface and concluded that the centrifugal mechanism was not important for their flow conditions. Floryan (2002) considered a formal linear stability analysis of Couette flow in the same geometry and identified conditions necessary for the generation of the vortices. The final example involves spatial flow modulation induced by Tollmien–Schlichting waves. Such waves may, under certain conditions, generate a secondary flow in the form of streamwise vortices, as postulated by Görtler & Witting (1958); this process is referred to as the secondary instability and the vortices are at present attributed to parametric resonance (Orszag & Patera 1983).

The examples discussed above exhibit differences in the sense that mean flow modulations are driven by different primary mechanisms. At the same time, these examples exhibit generic similarities in the sense that streamwise flow periodicity leads to the formation of streamwise vortices. Each case involves different distributions of the mean flow shear and streamline curvature and thus predictions regarding the formation of the vortices widely vary, if available at all. The mechanisms that may contribute to the creation of the vortices include centrifugal forces, the CL1 and CL2 mechanisms, and parametric resonance. The present study considers another source of flow modulation, i.e. wall transpiration, and the resulting combination of

the mean flow shear and streamline geometry is unlike the ones studied before and thus warrants a separate investigation. It is argued that the vortices considered here are driven by the centrifugal effect with the other mechanisms, which cannot be in general excluded, playing a complementary role.

The characterization of the centrifugal force field created by wall transpiration is difficult as this field is a function of the spatial distribution of the transpiration. The character of the force field may change between destabilizing and stabilizing for various segments of the flow field. The critical conditions for the occurrence of the instability, which must include characterization of the spatial distribution of the transpiration, are sought. The distribution of transpiration that could potentially lead to the instability does not need to be unique. In the present study, this distribution is represented in terms of Fourier expansions. Detailed results are presented for distributions described by a single Fourier mode, which can be characterized by two parameters, i.e. the amplitude and the wavelength of the transpiration. It is expected that the flow may become unstable for various combinations of these two parameters with the value of the critical Reynolds number being different in each case. The global critical Reynolds number, where the flow does not become unstable with respect to streamwise vortices for the specified amplitude of the transpiration regardless of its wavelength, is also sought.

This paper is organized as follows. Section 2 gives description of plane Couette flow modified by wall transpiration. Section 3 discusses linear stability of this flow. Section 4 is a discussion of the results. Section 5 gives a short summary of the main conclusions.

2. Couette flow with suction

2.1. *Problem formulation*

This section describes modifications of the plane Couette flow induced by application of wall transpiration.

Consider plane Couette flow confined between flat rigid walls at $y=\pm 1$ and extending to $\pm\infty$ in the x-direction. The velocity and pressure fields have the form

$$\boldsymbol{v}_0(x, y) = [u_0(y), 0] = [(y+1)/2, 0], \quad p_0(x, y) = \text{const}, \tag{2.1}$$

where the fluid motion is directed towards the positive x-axis. The motion of the upper wall drives the flow while the lower wall is stationary. The relevant Reynolds number Re is based on the velocity of the upper wall and the half-channel height.

At the lower wall transpiration is applied, leading to boundary conditions in the form

$$u(x, -1) = 0, \quad v(x, -1) = v_L(x), \tag{2.2a,b}$$

$$u(x, 1) = 0, \quad v(x, 1) = 0, \tag{2.2c,d}$$

where the subscript L refers to the lower wall. We shall restrict the analysis to transpiration that is periodic in x with the wavelength $\lambda_x = 2\pi/\alpha$. The transpiration distribution can be expressed in terms of Fourier series in the form

$$v_L(x) = \sum_{n=-\infty}^{n=\infty} V_n \mathrm{e}^{\mathrm{i}n\alpha x}, \tag{2.3}$$

where $V_n = V_n^*$ in order for v_L to be real. Here, an asterisk denotes complex conjugate. We shall assume that $V_0 = 0$, i.e. the transpiration on average carries zero mass flux.

The velocity and pressure fields can be represented as

$$\boldsymbol{v}(x, y) = [u_0(y), 0] + [u_1(x, y), v_1(x, y)], \quad p(x, y) = \text{const} + p_1(x, y), \tag{2.4}$$

where u_1, v_1 and p_1 are the velocity and pressure modifications due to the presence of wall transpiration. Substitution of the above representation of the flow quantities into the Navier–Stokes and continuity equations, introduction of stream function defined as

$$u_1 = \partial_y \Psi, \quad v_1 = -\partial_x \Psi \tag{2.5}$$

and elimination of pressure permits the field equations to be expressed in the form

$$(u_0 \partial_x + \partial_y \Psi \partial_x - \partial_x \Psi \partial_y) \nabla \Psi = \frac{1}{Re} \nabla^2 \Psi, \tag{2.6}$$

where ∇ denotes Laplace operator, ∂ denotes partial differentiation, and subscripts x and y denote the arguments of partial differentiations.

Since u_1 and v_1 are periodic in x with period $\lambda_x = 2\pi/\alpha$, the stream function can be represented as

$$\Psi(x, y) = \sum_{n=-\infty}^{n=+\infty} \Phi_n(y) \mathrm{e}^{\mathrm{i}n\alpha x}, \tag{2.7}$$

where $\Phi_n = \Phi^*_{-n}$. Substitution of (2.7) into (2.6) and separation of Fourier components leads to the following equation for Φ_n, $n \geqslant 0$:

$$\left[\mathrm{D}_n^2 - \mathrm{i}n\alpha Re u_0 \mathrm{D}_n\right] \Phi_n - \mathrm{i}\alpha Re \sum_{k=-\infty}^{k=+\infty} [k \mathrm{D}\Phi_{n-k} \mathrm{D}_k \Phi_k - (n-k) \Phi_{n-k} \mathrm{D}_k \mathrm{D} \Phi_k] = 0, \tag{2.8}$$

where $\mathrm{D}_n = \mathrm{D}^2 - n^2\alpha^2$ and $\mathrm{D} = \mathrm{d}/\mathrm{d}y$. The relevant boundary conditions have the form

$$\left.\begin{aligned} &\mathrm{D}\Phi_n(-1) = \mathrm{D}\Phi_n(1) = 0, \quad n \geqslant 0, \\ &\Phi_n(-1) = \mathrm{i}V_n/n\alpha, \quad \Phi_n(1) = 0, \quad n \geqslant 1. \end{aligned}\right\} \tag{2.9a}$$

It is assumed that presence of wall transpiration does not affect the mass flux through the channel, which leads to additional conditions in the form (Floryan 1997)

$$\Phi_0(-1) = 0, \quad \Phi_0(1) = 0 \tag{2.9b}$$

that are required to close problem formulation. The first condition in (2.9b) has been selected arbitrarily without loss of generality.

The pressure field associated with flow modifications can be expressed as

$$\frac{\partial p_1}{\partial x} = \sum_{n=-\infty}^{n=\infty} P_n(y) \mathrm{e}^{\mathrm{i}n\alpha x}. \tag{2.10a}$$

The change in the mean streamwise pressure gradient induced by the transpiration can be evaluated as (Floryan 1997)

$$P_0 = \frac{1}{2Re} \left(\left.\frac{\mathrm{d}^2 \Phi_0}{\mathrm{d}y^2}\right|_{y=1} - \left.\frac{\mathrm{d}^2 \Phi_0}{\mathrm{d}y^2}\right|_{y=-1} \right). \tag{2.10b}$$

The energy E_n of the nth mode is defined as

$$E_0 = \frac{1}{4} \int_{-1}^{1} |\bar{v}_{0n}|^2 \mathrm{d}y, \quad E_n = \frac{1}{2} \int_{-1}^{1} |\bar{v}_{1n}|^2 \mathrm{d}y, \quad n \neq 0 \tag{2.11}$$

where $\bar{v}_{1n}$ stands for the velocity vector corresponding to the nth term in (2.7).

2.2. *The numerical solution*

The problem to be solved consists of an infinite system of nonlinear ordinary differential equations (2.8) subject to boundary conditions (2.9). This section briefly describes the solution procedure.

As a first step, the representation of the stream function of the flow modifications Ψ is truncated to the M leading Fourier modes, i.e.

$$\Psi(x, y) \approx \sum_{n=-M}^{n=M} \Phi_n(y) \mathrm{e}^{\mathrm{i}n\alpha x}. \tag{2.12}$$

The corresponding finite-dimensional system of ordinary differential equations for the functions $\Phi_n, n = 0, 1, \ldots, M$, can be easily written on the basis of equations (2.10). This system can be discretized by introducing Chebyshev representations of the unknown function Φ_n in the form

$$\Phi_n(y) = \sum_{j=0}^{j=\infty} G_j^n T_j(y) \approx \sum_{j=0}^{j=K} G_j^n T_j(y), \tag{2.13}$$

where T_j denotes the Chebyshev polynomial of the jth order, G_j^n stands for the unknown expansion coefficient and the expansions are limited to the first $K + 1$ polynomials for calculation purposes. The Chebyshev representations of the required derivatives $\mathrm{D}^m\Phi$ (with m up to 4) can be determined using a recursive algorithm described by Canuto *et al.* (1988).

The nth equation of our system can be written in the general form

$$\Xi_n(\Phi_0, \Phi_1, \ldots, \Phi_M) = 0 \quad \text{for} \quad n = 0, \ldots, M. \tag{2.14}$$

The substitution of the Chebyshev expansions (2.13) and their derivatives into (2.14) gives the residual function

$$R_n = \Xi_n \left(\sum_{j=0}^{j=K} G_j^0 T_j, \sum_{j=0}^{j=K} G_j^1 T_j, \ldots, \sum_{j=0}^{j=K} G_j^M T_j \right), \quad n = 0, \ldots, M. \tag{2.15}$$

The problem is converted to an algebraic, nonlinear system by imposing the orthogonality conditions

$$\langle R_n, T_j \rangle_\omega = 0, \quad j = 0, \ldots, K - 4, \quad n = 0, \ldots, M. \tag{2.16}$$

where the inner product is defined as

$$\langle f, g \rangle_\omega := \int_{-1}^{1} f(y) g(y) \omega(y) \, \mathrm{d}y, \quad \omega(y) = (1 - y^2)^{-1/2}.$$

The discretization method described above can be viewed as a variant of the Chebyshev–tau technique. The reader should note that the projection is carried out onto the linear subspace spanned by the Chebyshev polynomials with the order of up to $K - 4$. The additional equations required to close the system are due to flow boundary conditions (2.9*a*) and volume flux conditions (2.9*b*). The results were spot-checked using the method described by Floryan (1997), which had been programmed separately. Appropriate selection of the discretization parameters as well as the overall accuracy of the numerical solution will be discussed in § 3.2.

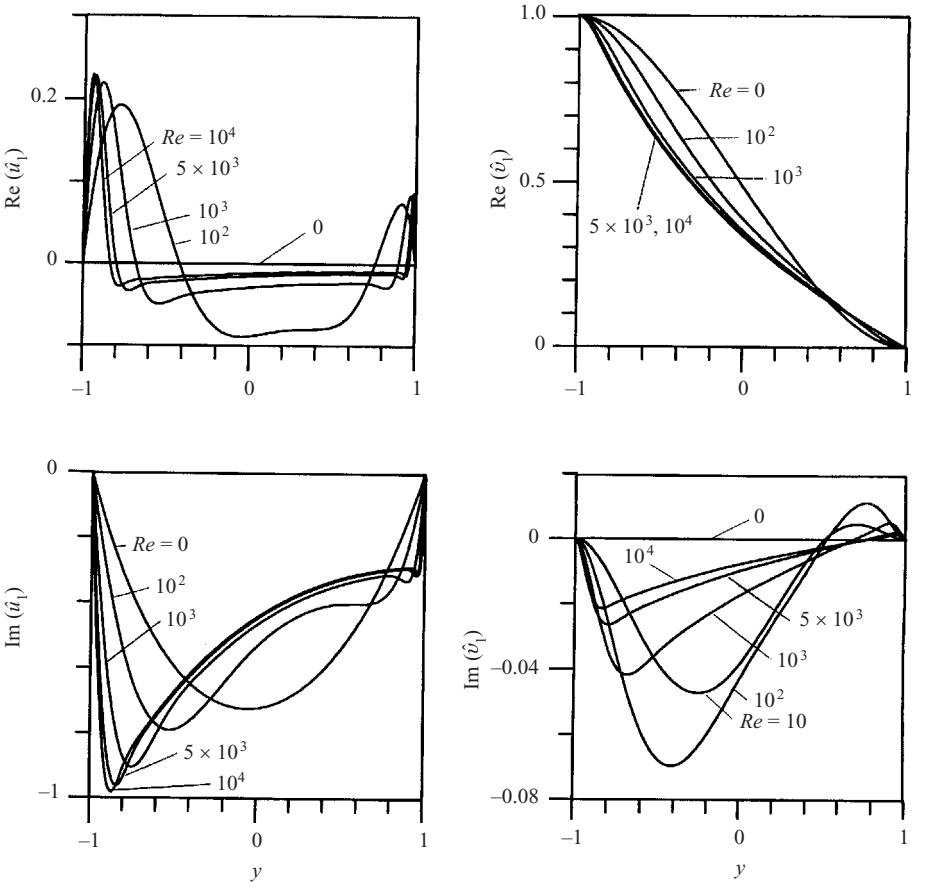

FIGURE 1. Modifications of Couette flow induced by the presence of wall transpiration as a function of the Reynolds number Re for transpiration wavenumber $\alpha = 1.0$ obtained with the linear model (§2.4). Hats denote quantities normalized with the amplitude of transpiration S resulting in $\hat{v}_1 = 1$ at $y = -1$.

2.3. *Linear model*

The linear model plays an important role, as will be established in §4, and so it warrants a separate discussion. For small suction amplitude, the nonlinear coupling between different modes in (2.7) becomes negligible. Under such circumstances, it is sufficient to consider wall suction in the form of a single Fourier harmonic, which leads to the following boundary value problem:

$$\{(\mathrm{D}^2 - \alpha^2)^2 - \mathrm{i}\alpha Re u_0(\mathrm{D}^2 - \alpha^2)\}\Phi_1 = 0, \tag{2.17a}$$

$$\Phi_1(-1) = \mathrm{i}S\alpha^{-1}, \quad \mathrm{D}\Phi_1|_{y=-1} = \Phi_1(1) = \mathrm{D}\Phi_1|_{y=1} = 0, \tag{2.17b}$$

where $S = V_1$. Special solutions of the above problem are described in Appendix A. Figures 1 and 2 illustrate velocity fields (normalized with factor S) for typical cases of interest. Results shown in figure 1 demonstrate that the character of the flow field modifications changes weakly as a function of the Reynolds number Re. Results shown in figure 2 demonstrate their rapid evolution as a function of the wavenumber α. The qualitative differences are underscored well in this case by the analytical forms

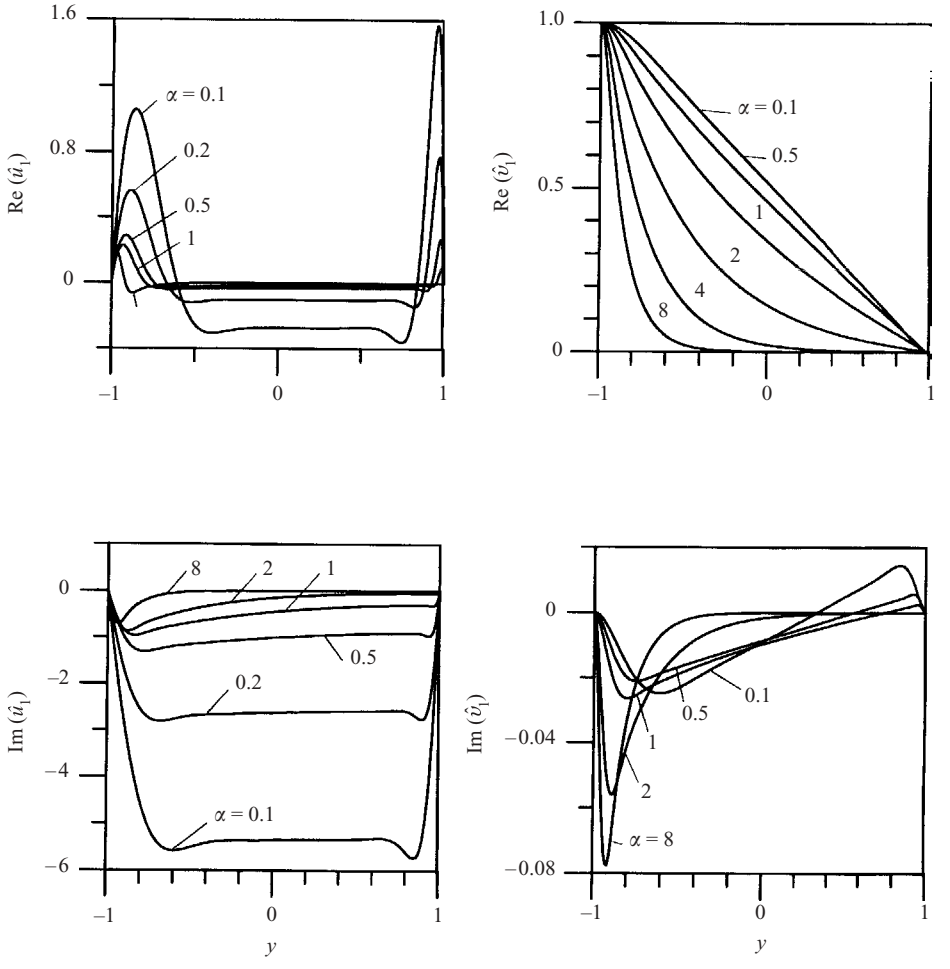

FIGURE 2. Modifications of Couette flow induced by the presence of wall transpiration as a function of the transpiration wavenumber α for $Re = 5000$. Other conditions as in figure 1.

of the solution in the limits of $\alpha \to 0$ and $\alpha \to \infty$ described in Appendix A. Limits of the applicability of the linear model can be judged on the basis of the results shown in figure 3. This figure displays variations of energies E_n of the first three modes as a function of the transpiration amplitude S. The energies were computed using the complete nonlinear model (2.8) truncated at $M = 7$. It can be seen that the nonlinear effects are negligible for approximately $S \leqslant 10^{-2}$. When the Reynolds number decreases, the magnitude of the transpiration amplitude for which the linear model is acceptable increases slightly. Additional comments regarding the applicability of the linear model are given in § 3.2.

3. Stability analysis

This section describes the linear stability analysis of Couette flow modified by wall transpiration using methodology developed by Floryan (1997).

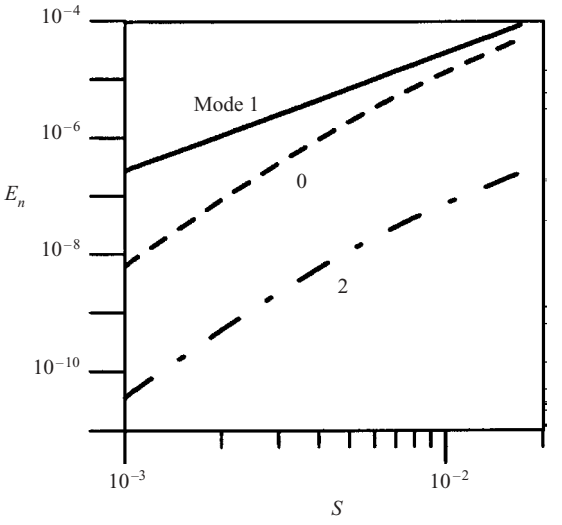

FIGURE 3. Energy E_n of the first three modes (see (2.11)) associated with the modifications of Couette flow induced by the wall transpiration in the form of a single Fourier mode with wavenumber $\alpha = 1$ for $Re = 5000$ as a function of the transpiration amplitude S.

3.1. *Problem formulation*

The analysis begins with the governing equations in the form of vorticity transport and continuity equations in the form

$$\frac{\partial \boldsymbol{\omega}}{\partial t} - (\boldsymbol{\omega}\cdot\nabla)\boldsymbol{v} + (\boldsymbol{v}\cdot\nabla)\boldsymbol{\omega} = \frac{1}{Re}\nabla^2\boldsymbol{\omega}, \quad \nabla\cdot\boldsymbol{v} = 0, \quad \boldsymbol{\omega} = \nabla\times\boldsymbol{v}. \tag{3.1a,b,c}$$

Unsteady three-dimensional disturbances are superimposed on the mean part in the form

$$\boldsymbol{\omega} = \boldsymbol{\omega}_2(x, y) + \boldsymbol{\omega}_3(x, y, z, t), \quad \boldsymbol{v} = \boldsymbol{v}_2(x, y) + \boldsymbol{v}_3(x, y, z, t), \tag{3.2}$$

where subscripts 2 and 3 refer to the mean flow and the disturbance field, respectively. The assumed form of the flow, (3.2), is substituted into (3.1), the mean part is subtracted and the equations are linearized. The resulting linear disturbance equations have the form

$$\frac{\partial \boldsymbol{\omega}_3}{\partial t} + (\boldsymbol{v}_2\cdot\nabla)\boldsymbol{\omega}_3 - (\boldsymbol{\omega}_3\cdot\nabla)\boldsymbol{v}_2 + (\boldsymbol{v}_3\cdot\nabla)\boldsymbol{\omega}_2 - (\boldsymbol{\omega}_2\cdot\nabla)\boldsymbol{v}_3 = \frac{1}{Re}\nabla^2\boldsymbol{\omega}_3, \tag{3.3a}$$

$$\nabla\cdot\boldsymbol{v}_3 = 0, \quad \boldsymbol{\omega}_3 = \nabla\times\boldsymbol{v}_3. \tag{3.3b,c}$$

The mean flow is assumed to have the form

$$\boldsymbol{v}_2(x, y) = [u_0(y), 0, 0] + \sum_{n=-\infty}^{n=\infty} \left[f_u^{(n)}(y), f_v^{(n)}(y), 0\right] \mathrm{e}^{\mathrm{i}n\alpha x} \tag{3.4}$$

where $f_u^{(n)}, f_v^{(n)}$ represent the solution to the problem (2.6)–(2.10) and $f_u^{(n)} = (f_u^{(-n)})^*$, $f_v^{(n)} = (f_v^{(-n)})^*$.

The disturbance equations (3.3) have coefficients that are functions of x and y only and thus the solution can be written in the form

$$\boldsymbol{v}_3(x, y, z, t) = \boldsymbol{h}_3(x, y)\mathrm{e}^{\mathrm{i}(\mu z - \sigma t)} + \text{c.c.} \tag{3.5}$$

where $\boldsymbol{h}_3 = (h_u, h_v, h_w)$. The exponent μ is real and accounts for the spanwise periodicity of the disturbance field. The exponent σ is assumed to be complex and its imaginary and real parts describe the rate of growth and the frequency of the disturbances, respectively.

The coefficients in (3.3) are periodic in x with periodicity $2\pi/\alpha$ and thus, in general, $\boldsymbol{h}_3$ should be written as

$$\boldsymbol{h}_3(x, y) = \mathrm{e}^{\mathrm{i}\delta x}\boldsymbol{g}_3(x, y) = \mathrm{e}^{\mathrm{i}\delta x}\sum_{m=-\infty}^{m=+\infty}\boldsymbol{G}^{(m)}(y)\mathrm{e}^{\mathrm{i}m\alpha x}, \tag{3.6}$$

where $\boldsymbol{g}_3$ is periodic in x with the same periodicity $2\pi/\alpha$ and δ is referred to as the Floquet exponent (Coddington & Levinson 1965). In the case of centrifugal instability, disturbances are expected to be in the form of streamwise vortices and thus the solution must include the non-periodic component. As a result, the Floquet exponent can be assumed to be zero without loss of generality. Nevertheless, this exponent is kept in the formulation and it is used to test the consistency and accuracy of the numerical solution. The final form of the disturbance velocity vector is written as

$$\boldsymbol{v}_3(x, y, z, t) = \sum_{m=-\infty}^{m=+\infty}\left[g_u^{(m)}(y), g_v^{(m)}(y), g_w^{(m)}(y)\right]\mathrm{e}^{\mathrm{i}[(\delta+m\alpha)x+\mu z-\sigma t]} + \text{c.c.} \tag{3.7}$$

Substitution of (3.4) and (3.7) into the disturbance equations (3.4) and separation of Fourier components results in a system of ordinary differential equations governing $g_u^{(m)}$, $g_v^{(m)}$, $g_w^{(m)}$ in the form

$$S^{(m)}\left(t_m g_w^{(m)} - \mu g_u^{(m)}\right) + C g_v^{(m)} = \mathrm{i}Re\sum_{n=-\infty}^{n=\infty}\left(W_u^{(m,n)}g_u^{(m-n)} + W_v^{(m,n)}g_v^{(m-n)} + W_w^{(m,n)}g_w^{(m-n)}\right), \tag{3.8a}$$

$$T^{(m)}g_v^{(m)} = -Re\sum_{n=-\infty}^{n=\infty}\left(B_u^{(m,n)}g_u^{(m-n)} + B_v^{(m,n)}g_v^{(m-n)} + B_w^{(m,n)}g_w^{(m-n)}\right), \tag{3.8b}$$

$$\mathrm{i}t_m g_u^{(m)} + \mathrm{D}g_v^{(m)} + \mathrm{i}\mu g_w^{(m)} = 0, \tag{3.8c}$$

where $\mathrm{D} = \mathrm{d}/\mathrm{d}y$, $t_m = m\alpha + \delta$ and the explicit forms of the operators T, S, C, W, B are given in the Appendix B. Equation (3.8*a*) describes the y-component of the disturbance vorticity, (3.8*b*) corresponds to $\mathrm{i}\mu \times (3.4a) - \mathrm{i}t_m \times (3.4c)$, and (3.8*c*) results from the continuity equation. It is convenient for analysis purposes to express the above relations in terms of the y-components of disturbance vorticity $\theta^{(m)} = t_m g_w^{(m)} - \mu g_u^{(m)}$ and disturbance velocity $g_v^{(m)}$, i.e.

$$S^{(m)}\theta^{(m)} + C g_v^{(m)} = Re\sum_{n=-\infty}^{n=\infty}\left(E_v^{(m,n)}g_v^{(m-n)} + E_\theta^{(m,n)}\theta^{(m-n)}\right), \tag{3.9a}$$

$$T^{(m)}g_v^{(m)} = -Re\sum_{n=-\infty}^{n=\infty}\left(H_v^{(m,n)}g_v^{(m-n)} + H_\theta^{(m,n)}\theta^{(m-n)}\right), \tag{3.9b}$$

where the explicit forms of the operators E, H are given in the Appendix B.

Effects of wall suction are contained in the terms on the right-hand side of (3.9). In their absence, all modes in the Fourier series (3.6) decouple and (3.9) describes the classical three-dimensional instability of ideal Couette flow. The coupling involves $2N+1$ consecutive terms from the Fourier series, where N describes the actual length

of the Fourier series in (3.4). In analogy to the stability of flow in a channel without wall transpiration, we shall refer to the T, S and C operators as the Tollmien–Schlichting, Squire and coupling operators, respectively. Operators E and H arise because of flow forcing due to the presence of wall transpiration and thus we shall refer to them as the forcing operators. E_θ and H_v describe direct forcing and E_v and H_θ describe coupling due to the forcing.

Equations (3.9), together with homogeneous boundary conditions, have non-trivial solutions only for certain combinations of parameters V_n, α, σ and μ. The required dispersion relation has to be determined numerically. Since interest here is in the temporal instability, the problem for numerical solution was posed as an eigenvalue problem for σ.

3.2. *Numerical solution*

The problem to be solved consists of an infinite system of ordinary differential equations (3.9) with homogeneous boundary conditions. Approximate solutions can be found by truncating the sum in (3.7) after a finite number L of terms and solving the eigenvalue problem for $2L+1$ differential equations of type (3.9). All calculations reported in this paper have been carried out for the wall transpiration in the form of a single Fourier mode with $V_1 = S$, $V_n = 0$ for $n \neq 1$ (see (2.3)).

The differential equations were discretized using a method similar to the one described in § 2.3. An alternative discretization method described by Floryan (1997) was also implemented and was used to spot-check the results.

The discretization procedure results in a matrix eigenvalue problem $\boldsymbol{\Omega} x = 0$ where $\boldsymbol{\Omega}(\sigma)$ represents the coefficient matrix. This matrix is linear in σ, i.e. $\boldsymbol{\Omega} = \boldsymbol{\Omega}_0 + \boldsymbol{\Omega}_1 \sigma$, where $\boldsymbol{\Omega}_0 = \boldsymbol{\Omega}(0)$, $\boldsymbol{\Omega}_1 = \boldsymbol{\Omega}(1) - \boldsymbol{\Omega}_0$. The σ-spectrum is determined by solving a general eigenvalue problem in the form $\boldsymbol{\Omega}_0 x = \sigma \boldsymbol{\Omega}_1 x$. The individual eigenvalues are determined by finding zeros of the determinant of $\boldsymbol{\Omega}$.

Two methods for tracing of eigenvalues in the parameter space have been used. In the first method, one alters flow conditions and produces an approximation for the eigenvalue, which is then improved iteratively by searching for the nearby zero of the determinant using a Newton–Raphson search procedure. In the second, the inverse iterations method, one computes an approximation for the eigenvector $\boldsymbol{\Lambda}_a$ corresponding to the unknown eigenvalue σ_a using an iterative process in the form $(\boldsymbol{\Omega}_0 - \sigma_0 \boldsymbol{\Omega}_1)\boldsymbol{\Lambda}^{(n+1)} = \boldsymbol{\Omega}_1 \boldsymbol{\Lambda}^{(n)}$ where σ_0 and $\boldsymbol{\Lambda}^{(0)}$ are the eigenvalue and the eigenvector (an eigenpair) corresponding to the unaltered flow. If σ_a is the eigenvalue closest to σ_0, $\boldsymbol{\Lambda}^{(n)}$ converges to $\boldsymbol{\Lambda}_a$. The eigenvalue σ_a is evaluated using formula $\sigma_a = \boldsymbol{\Lambda}_a^* \boldsymbol{\Omega}_0 \boldsymbol{\Lambda}_a / \boldsymbol{\Lambda}_a^* \boldsymbol{\Omega}_1 \boldsymbol{\Lambda}_a$ where the asterisk denotes the complex-conjugate transpose. The inverse iterations method was found to be generally more efficient.

Results of numerical tests presented in tables 1–4 dealing with numerical evaluation of eigenvalue σ assist in identifying the correct settings of various numerical parameters. These tests deal with the flow conditions around the onset of the instability. Tables 1 and 2 shows that in the case of a medium Reynolds number of $Re = 5000$ eigenvalues can be determined with accuracy no worse then 1% using $K = 39$ Chebyshev polynomials, $M = 1$ Fourier modes to represent the base flow and $L = 1$ Fourier modes to represent the disturbances. This demonstrates that the linear model of flow modifications discussed in § 2.3 is relevant for such flow conditions. Results displayed in tables 3 and 4 for small Reynolds number $Re = 182$ demonstrate that one needs to use $M = 3$ Fourier modes to represent base flow, $L = 3$ Fourier modes to represent disturbances and $K = 39$ Chebyshev polynomials

L – number of Fourier modes used to represent disturbances	Number of base flow Fourier modes retained in the stability equations	M – number of Fourier modes used in the base flow solution		
		1	2	3
1	1	1.266942	1.267717	1.267049
2	1	1.257439	1.257659	1.257542
	2		1.257682	1.257564
3	1	1.257442	1.257662	1.257545
	2		1.257693	1.257575
	3			1.257570

TABLE 1. Disturbance amplification rate $\mathrm{Im}(\sigma) \times 10^3$ for the transpiration amplitude $S = 0.0015$, the transpiration wavenumber $\alpha = 1$, the flow Reynolds number $Re = 5 \times 10^3$ and the vortex wavenumber $\mu = 1$ obtained using $K = 59$ Chebyshev polynomials.

Number of Chebyshev polynomials	39	49	59
$\mathrm{Im}(\sigma) \times 10^3$	1.257570	1.257570	1.257570

TABLE 2. Disturbance amplification rate $\mathrm{Im}(\sigma)$ for the transpiration amplitude $S = 0.0015$, the transpiration wavenumber $\alpha = 1$, the flow Reynolds number $Re = 5 \times 10^3$ and the vortex wavenumber $\mu = 1$ obtained using $M = L = 3$ Fourier modes to represent the base flow and the disturbance field.

L – number of Fourier used to represent disturbances	Number of base flow Fourier modes retained in the stability equations	M – number of Fourier modes used in the base flow solution		
		3	5	7
3	3	0.312755	0.320822	0.320846
5	3	0.315098	0.322809	0.322833
	5		0.322532	0.322599
7	3	0.315170	0.322878	0.322901
	5		0.322600	0.322667
	7			0.322657

TABLE 3. Disturbance amplification rate $\mathrm{Im}(\sigma) \times 10^3$ for the transpiration amplitude $S = 0.05$, the transpiration wavenumber $\alpha = 1.1$, the flow Reynolds number $Re = 182$ and the vortex wavenumber $\mu = 1.75$ obtained using $K = 59$ Chebyshev polynomials.

Number of Chebyshev polynomials	39	49	59
$\mathrm{Im}(\sigma) \times 10^3$	0.322657	0.322657	0.322657

TABLE 4. Disturbance amplification rate $\mathrm{Im}(\sigma)$ for the suction amplitude $S = 0.05$, the suction wavenumber $\alpha = 1.1$, the flow Reynolds number $Re = 182$ and the vortex wavenumber $\mu = 1.75$ obtained using $M = L = 7$ Fourier modes to represent the base flow and the disturbance field.

to get the same accuracy of 1%. The higher accuracy requirements in this case result primarily from the fact that the instability occurs at higher values of the transpiration amplitude.

Note that in the case of disturbances in the form of streamwise vortices, the x- and y-components of $\boldsymbol{G}^{(m)}$ in (3.6) are real, the z-component is imaginary, i.e. $g_u^{(m)} = g_u^{(-m)^*}$, $g_v^{(m)} = g_v^{(-m)^*}$, $g_w^{(m)} = -g_w^{(-m)^*}$, the exponent σ is imaginary, and the size of the system to be solved numerically can be decreased by the ratio $(2M+1)/(M+1)$. This is equivalent to the formulation of the stability problem in terms of real rather than complex variables. In this work a general problem has been solved numerically and special properties of the solution have been used for verification of the consistency of the results. The availability of Floquet exponent δ has also been used for numerical verification of certain properties of the solution. All theoretically expected properties have been reproduced numerically.

4. Discussion of results

The following discussion is focused on the temporal stability theory, i.e. the exponent σ is complex and its imaginary part describes the rate of growth of disturbances. All results deal with plane Couette flow modified by transpiration in the form of a single Fourier mode. The transpiration is applied at the bottom wall only, its amplitude S is assumed to be real and the resulting normal velocity distribution has the form $v_L(x) = 2S\cos(\alpha x)$.

Ideal Couette flow is linearly stable (Romanov 1972). Results of this analysis show that the presence of wall transpiration leads to the appearance of growing disturbances at finite Reynolds numbers. This particular study is focused on disturbances in the form of streamwise vortices and thus the dominant mode corresponds to $m = 0$ in (3.7). The vortices are modulated in the streamwise direction with the same periodicity as that of the transpiration, i.e. the wavelength of the modulations is $2\pi/\alpha$. The stability analysis is linear and permits determination of critical conditions only. The flow evolution past the critical conditions requires a fully nonlinear analysis, as the presence of vortices produces large changes in the mean flow (Benmalek & Saric 1994).

4.1. *Instability in the case of medium Reynolds numbers*

It is useful to begin this discussion with a description of the form of the base flow. Figure 4(*a*) illustrates the form of streamlines for $Re = 5000, \alpha = 1, S = 0.0015$. Wall transpiration produces bubbles containing fluid transferred through the wall. These bubbles displace the fluid already in the channel, forcing it to change direction in order to flow around them. The distribution of the resulting streamline curvature, which can be evaluated according to the formula

$$K = \left(u_1^2 \frac{\partial v_1}{\partial x} - v_1^2 \frac{\partial u_1}{\partial y} - 2 v_1 u_1 \frac{\partial u_1}{\partial x} \right) \Big/ \left(v_1^2 + u_1^2 \right)^{3/2}, \tag{4.1}$$

is illustrated in figure 4(*b*). The curvature is negative over approximately the first half of the period in the x-direction, and positive over the second half. Potential for instability driven by centrifugal effect is expressed in terms of the Rayleigh criterion (Rayleigh 1916; Drazin & Reid 1981) that states that a necessary and sufficient condition for stability is that the square of the circulation should not decrease anywhere. This criterion had been derived in the case of flow between circular cylinders using a polar system of coordinates where the positive direction is uniquely defined. In the present case the flow is described in terms of a Cartesian system and thus the positive direction corresponds to increasing y in the area where the

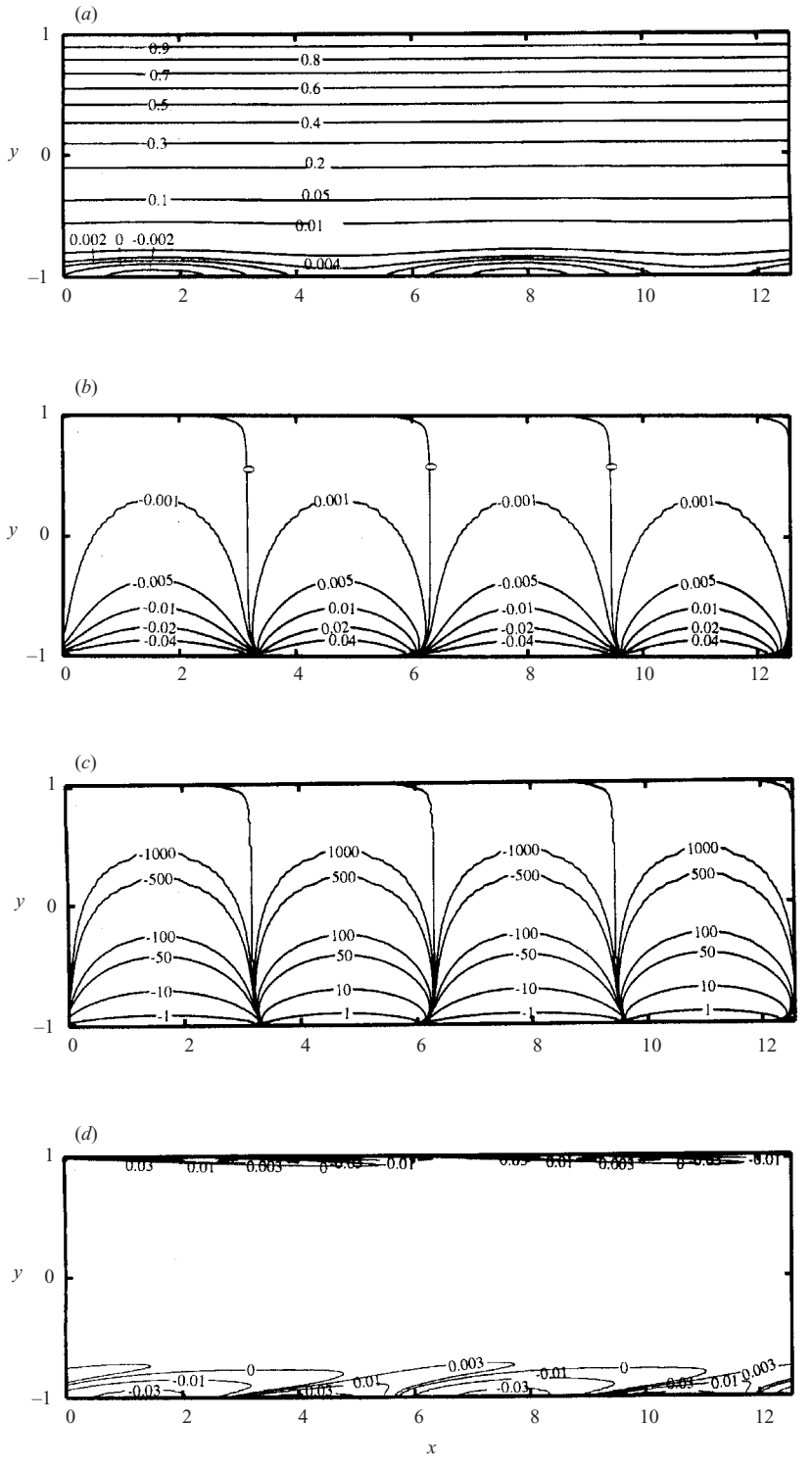

FIGURE 4. Form of base flow resulting from the presence of transpiration with wavenumber $\alpha = 1$ and amplitude $S = 0.0015$ for $Re = 5000$ and $x \in (0, 4\pi/\alpha)$: (*a–d*) display streamline pattern, streamline curvature, circulation and vorticity, respectively.

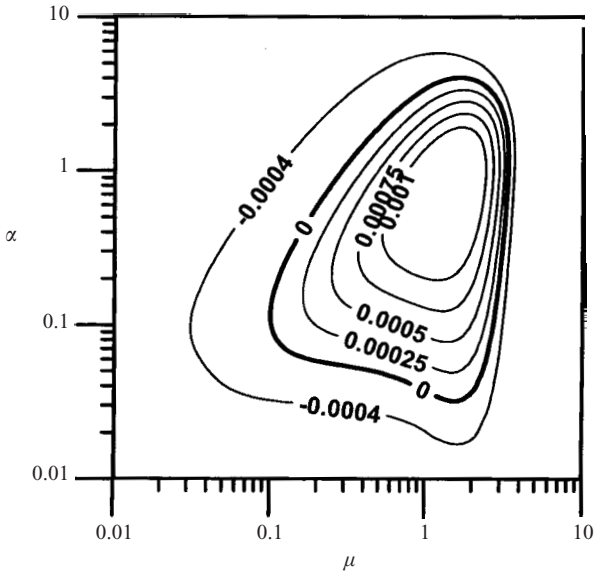

FIGURE 5. Amplification rate $\mathrm{Im}(\sigma)$ of disturbances in the form of streamwise vortices induced by wall transpiration in the form of a single Fourier mode with amplitude $S = 0.0015$ for $Re = 5000$ as a function of the vortex wavenumber μ and the transpiration wavenumber α.

curvature is negative, and decreasing y in the area where the curvature is positive. The circulation can be evaluated according to the formula

$$\Gamma = (|\boldsymbol{v}|/K) = \left(v_1^2 + u_1^2\right)^2 \Big/ \left(u_1^2 \frac{\partial v_1}{\partial x} - v_1^2 \frac{\partial u_1}{\partial y} - 2v_1 u_1 \frac{\partial u_1}{\partial x}\right) \tag{4.2}$$

and its distribution is illustrated in figure 4(c). It can be seen that the flow violates the Rayleigh criterion in the zone corresponding approximately to the second half of the flow period in the x-direction. Figure 4(d) illustrates the distribution of vorticity in the base flow. It can be seen that the transpiration acts as a source of vorticity at the lower as well as upper walls. The presence of such a vorticity source may lead to interesting dynamics of turbulent Couette flow.

Results of the full linear stability analysis are illustrated in figure 5, which displays the amplification rate $\mathrm{Im}(\sigma)$ of the vortices as a function of the transpiration wavenumber α for the flow Reynolds number $Re = 5000$ and the transpiration amplitude $S = 0.0015$. It can be seen that there is a finite range of transpiration wavenumbers α, bounded from above and from below, that gives rise to the instability. Each (unstable) transpiration wavenumber gives rise to growth of a continuous, finite band of vortices whose spanwise wavenumber μ is also bounded from above and from below. The neutral curve, which delineates the range of unstable (α, μ), is marked using a thicker line.

The occurrence of the instability identified above leads to a rapid three-dimensionalization of the flow field through the formation of streamwise streaks. It is known that such streaks play an important role in the transition process (Reddy *et al.* 1998; Waleffe 1997). Numerical simulations carried out by Floryan, Yamamoto & Murase (1992) show that a similar instability represents the initial stages of the bypass route to transition in the case of Poiseuille flow modified by suction. Qualitative

similarities between both instabilities suggest that surface transpiration may initiate a process leading to transition in the case of Couette flow also.

Figure 6 illustrates the form of the first three eigenfunctions associated with the vortices for $\mu = 1, \alpha = 1, S = 0.015$ and $Re = 5000$. The dominant character of $g_u^{(0)}$, which is a characteristic feature of the vortices, is clearly visible. The topology of the vortices is rather complex, as indicated by the form of the velocity 'amplitude function' $\boldsymbol{h}_3(x, y)$ displayed in figure 7. This complexity is associated with the streamwise modulation of the vortex. The disturbance velocity field topology is illustrated well by plots of transverse velocity vector in the (y, z)-plane displayed in figure 8. One pair of counter-rotating vortices can be seen at $x = 0$ (figure 8*a*). A second layer of vortices can be seen forming at the bottom of the channel at $x = \lambda/8$ (figure 8*b*). Here λ denotes the wavelength of the transpiration. This second layer is well-developed at $x = \lambda/4$ (figure 8*c*). The lower vortices are replaced at $x = 3\lambda/8$ by a one-dimensional jet-like structure directing the fluid away from $z = \pi/\mu$ (figure 8*d*). There is no vortex structure at all in the whole channel at $x = \lambda/2$ (figure 8*e*); it is replaced by one-dimensional flow in the same direction as at $x = 3\lambda/8$ with a distinct jet-like structure clearly visible at the bottom of the channel. Vortex structure in the centre of the channel re-emerges at $x = 5\lambda/8$ and it is accompanied by the same jet-like structure around the lower wall (figure 8*f*). A single layer of counter-rotating vortices is visible at $x = 3\lambda/4$ (figure 8*g*) with the jet-like structure at the bottom flowing in the opposite direction compared to $x = 5\lambda/8$. The formation of a more regular system of two counter-rotating vortices can be seen at $x = 7\lambda/8$ (figure 8*h*).

Flow patterns shown in figure 8(*d–g*) suggest the existence of apparent sinks and sources around the bottom of the channel at $z = 0, \pi/\mu$ and $2\pi/\mu$. This effect is associated with the streamwise modulation of the vortices and can explained by looking at the form of eigenfunctions displayed in figure 6. It can be seen that higher Fourier modes play a significant role near the bottom of the channel, especially for the y and z disturbance velocity components. The 'sink/source' effect is associated with the higher Fourier modes whose presence results in the local increase/decrease of the u velocity at different x-locations.

Figure 9 illustrates changes of the vortex amplification rate as a function of the amplitude S of the transpiration for a few selected vortices in the limit as $S \to 0$. The distinct limit $S = 0$ corresponds to Squire's mode and can be determined analytically, i.e. $\sigma = -\mathrm{i}(\mu^2 + \pi^2/4)/Re$ (Floryan 2002). The available results demonstrate that the part of the spectrum describing vortices is connected to Squire's spectrum in the absence of transpiration. The evolution of the $g_u^{(0)}$ eigenfunction with amplitude S is shown in figure 10 for $\alpha = 1, \mu = 1, Re = 5000$. The reader may note that disturbances have no streamwise vorticity when $S = 0$. Such vorticity may be viewed as being created by 'bending' of the plane vortex sheets by wall transpiration (figure 4*a*).

Figures 11, 12 and 13 display the eigenfuntions, the amplitude function $\boldsymbol{h}_3(x, y)$ and the transverse velocity fields, respectively, for $S = 0.0001$ and for the same values of α, μ and Re. These results permit analysis of transition of the disturbance velocity field from that corresponding to a stable vortex to an unstable one (figures 6, 7, 8). The shape of the eigenfunctions is similar for $S = 0.0015$ and $S = 0.0001$, with the higher modes being significantly smaller in the latter case. There are no vortices in a significant streamwise section of the channel, as shown in figure 12. The process of creation and elimination of vortices can be easily followed in figure 13. One pair of vortices can be seen in the upper section of the channel at $x = 0$ (figure 13*a*), while the lower two-thirds is occupied by the jet-like structure. A second layer of the vortices appears at $x = \lambda/8$ (figure 13*b*) while a very thin jet-like structure still

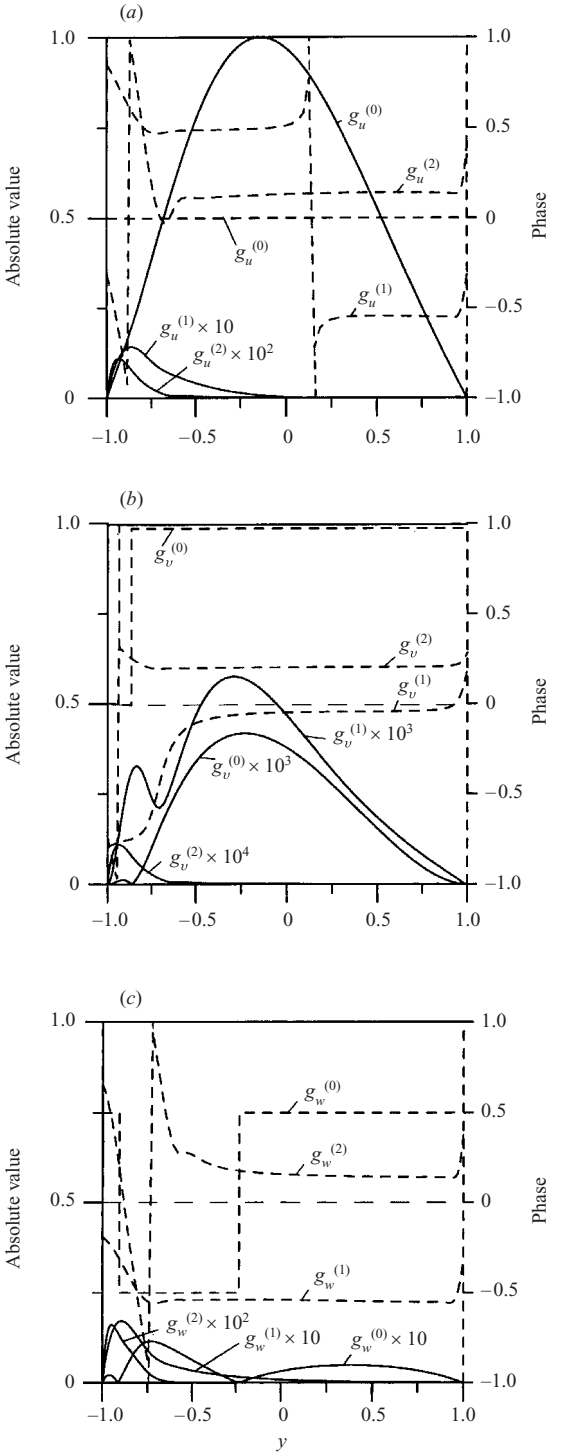

FIGURE 6. Eigenfunctions $g_u^{(m)}, g_v^{(m)}, g_w^{(m)}, m = 0, 1, 2$, describing a vortex with wavenumber $\mu = 1$ induced by the wall transpiration with wavenumber $\alpha = 1$ and amplitude $S = 0.0015$ for the flow Reynolds number $Re = 5000$ and normalized with condition $\max(g_u^{(0)}) = 1$. (*a–c*) Functions $g_u^{(m)}, g_v^{(m)}, g_w^{(m)}$, respectively.

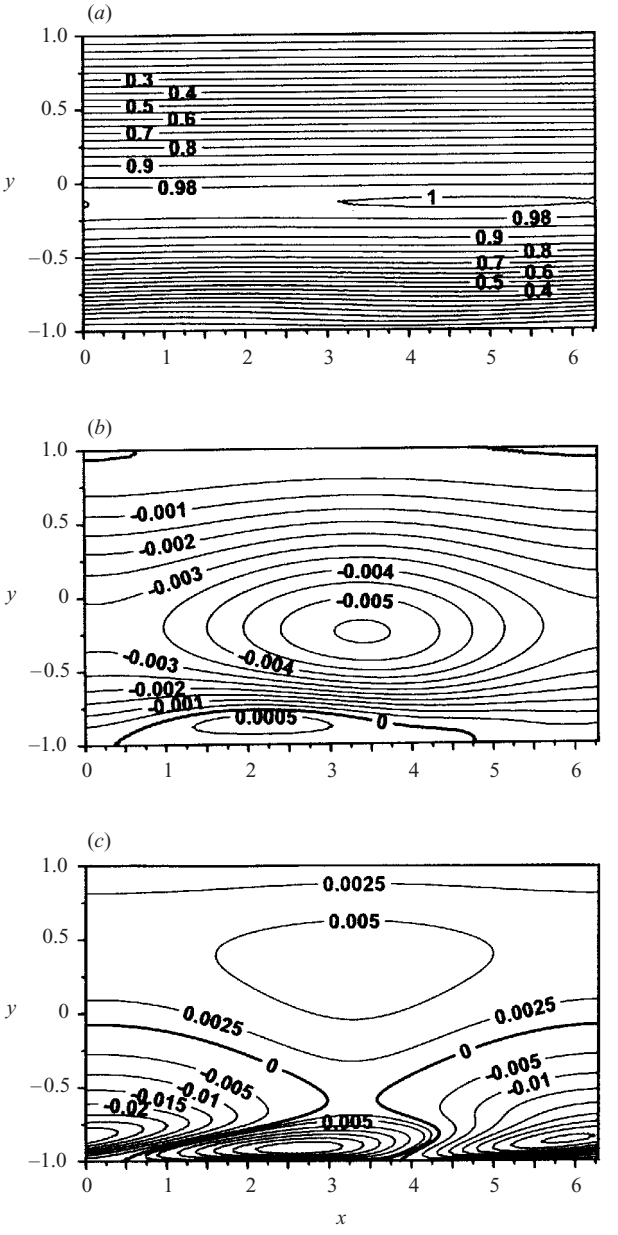

FIGURE 7. Velocity 'amplitude function' $\boldsymbol{h}_3(x, y) = [h_u(x, y), h_v(x, y), \mathrm{i}\hat{h}_w(x, y)]$ (see (3.5)) for $Re = 5000$, $\alpha = 1$, $\mu = 1$, $S = 0.0015$ normalized with condition $\max(g_u^{(0)}) = 1$. Functions h_u, h_v, $\hat{h}_w$ are displayed in (*a–c*), respectively.

exists at the bottom. The second layer grows and occupies most of the channel at $x = \lambda/4$ (figure 13*c*) while the first layer disappears altogether; the jet-like structure at the bottom begins to grow. This jet-like structure eliminates vortices and fills the whole channel at $x = 3\lambda/8$, $x = \lambda/2$ and $x = 5\lambda/8$ (figure. 13*d–f*). One may note the appearance of another jet-like structure flowing in the opposite direction at the bottom at $x = 5\lambda/8$ (figure 13*f*). Vortices re-appear at $x = 3\lambda/4$ (figure 13*g*)

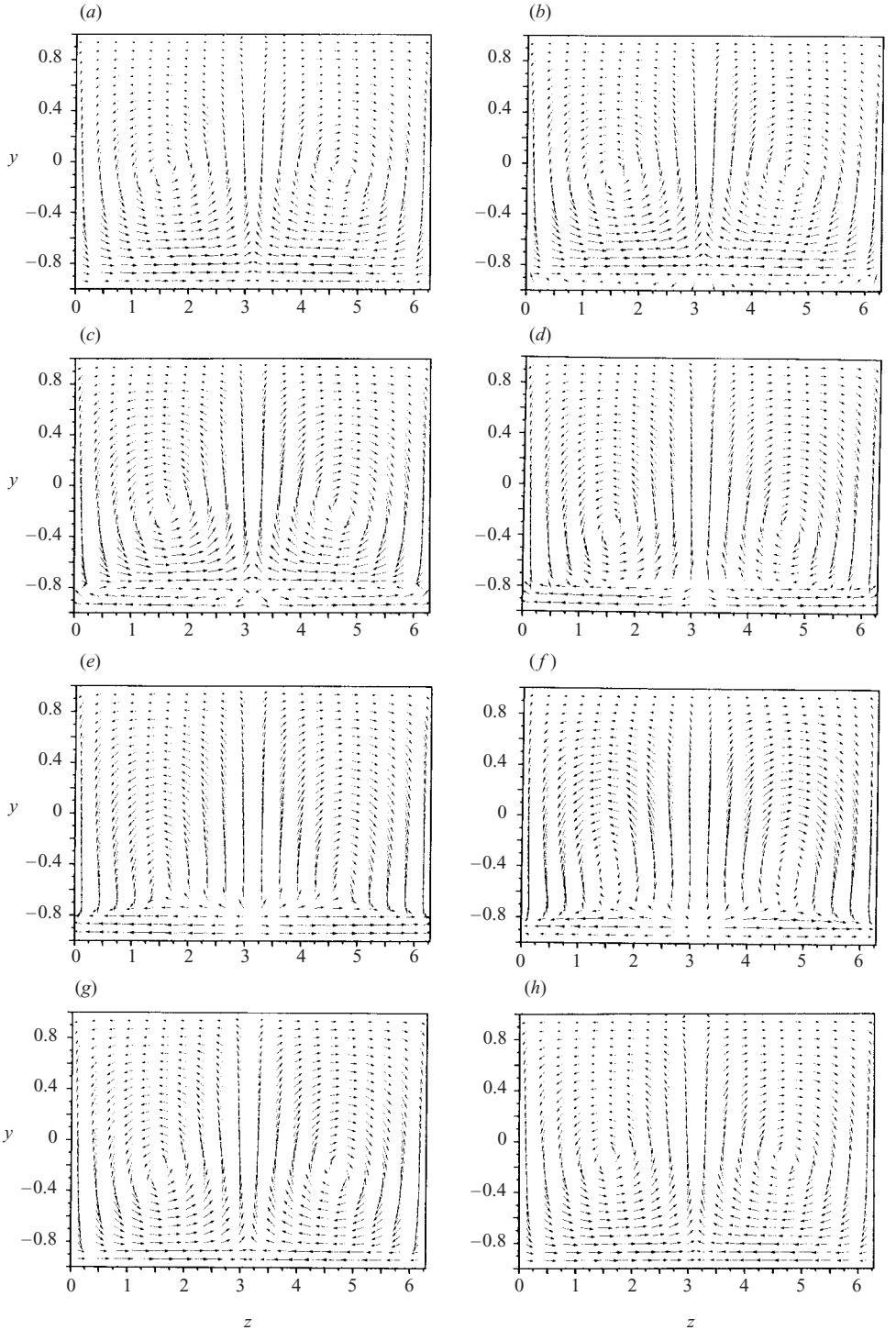

FIGURE 8. Distribution of the (y, z) component of the disturbance velocity vector for $z \in (0, 2\pi/\mu)$, $\mu = 1$, $\alpha = 1$, $Re = 5000$, $S = 0.0015$. The disturbance velocity vector is normalized with condition $\max(g_u^{(0)}) = 1$. (*a–h*) Correspond to $x = 0, \lambda/8, \lambda/4, 3\lambda/8, \lambda/2, 5\lambda/8, 3\lambda/4, 7\lambda/8$, respectively, where $\lambda = 2\pi/\alpha$ denotes one wavelength of wall transpiration.

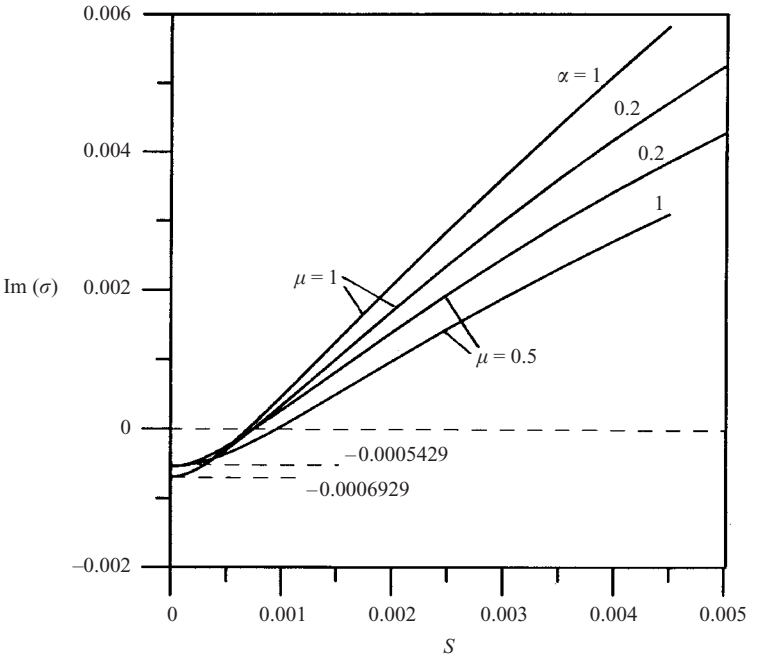

FIGURE 9. Variations of the amplification rate $\mathrm{Im}(\sigma)$ of streamwise vortices with wavenumber $\mu = 0.5$ and $\mu = 1$ induced by the wall transpiration with wavenumber $\alpha = 0.2$ and $\alpha = 1$ for $Re = 5000$ as a function of the transpiration amplitude S.

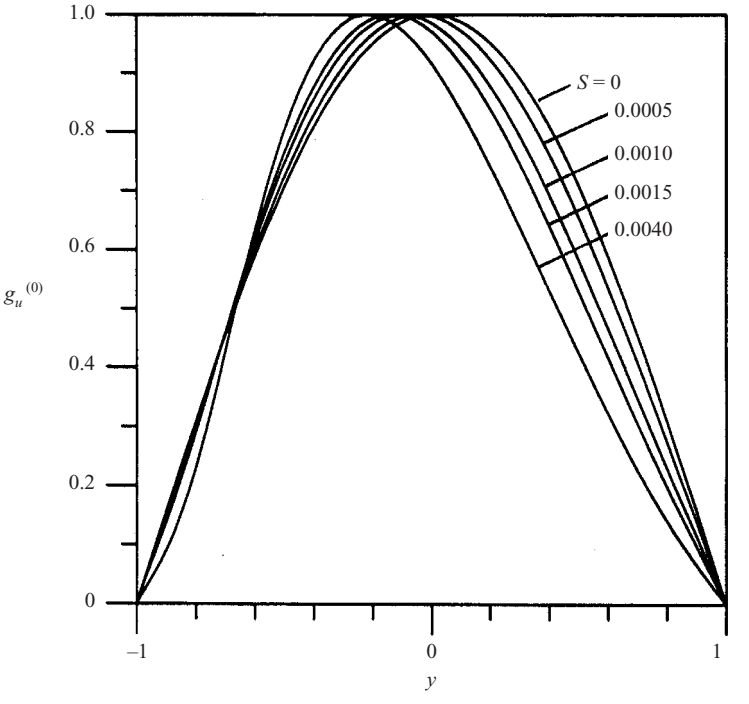

FIGURE 10. Evolution of the real part of the eigenfunction $g_u^{(0)}$ as a function of the transpiration amplitude S for $\alpha = 1$, $\mu = 1$, $Re = 5000$. Normalization condition $\max(g_u^{(0)}) = 1$. Since $g_u^{(0)}$ is real and positive, only $|g_u^{(0)}|$ is shown.

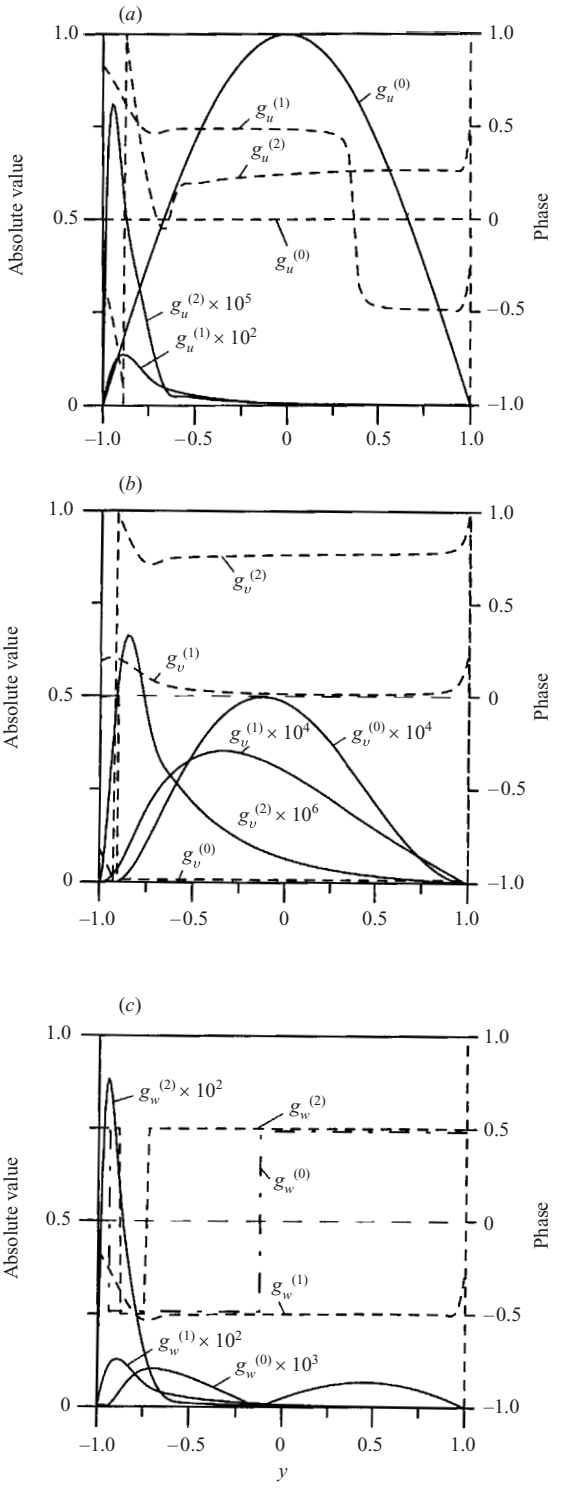

FIGURE 11. Eigenfunctions $g_u^{(m)}$, $g_v^{(m)}$, $g_w^{(m)}$, $m = 0, 1, 2$, describing a vortex with wavenumber $\mu = 1$ induced by wall transpiration with amplitude $S = 0.0001$. The remaining conditions are the same as those used in figure 6. (*a–c*) Functions $g_u^{(m)}$, $g_v^{(m)}$, $g_w^{(m)}$, respectively.

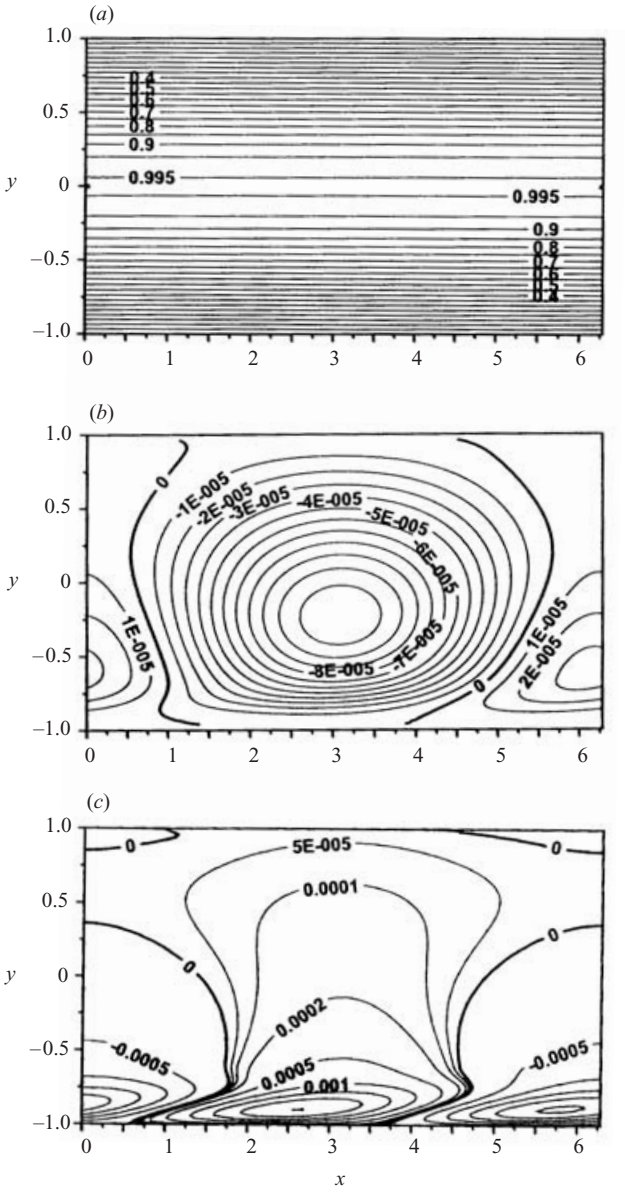

FIGURE 12. Velocity amplitude function $\boldsymbol{h}_3(x, y) = [h_u(x, y), h_v(x, y), \mathrm{i}\hat{h}_w(x, y)]$ (see (3.5)) for $S = 0.0001$. The remaining conditions are the same as those used in figure 7. Functions $h_u, h_v, \hat{h}_w$ are displayed in (*a–c*), respectively.

and fill the channel completely at $x = 7\lambda/8$ (figure 13*h*). One should note that the cross-sections (*g*), (*h*), (*a*) correspond to the zone where the fluid exits from between the 'bubbles' (streamlines begin to converge, i.e. figure 4*a*) and the centrifugal forces create vortices. The cross-sections (*d*), (*e*), (*f*) correspond to the zone where the fluid enters the area between the 'bubbles' (streamlines diverge, i.e. figure 4*a*). There is some vortex re-arrangement at the cross-sections (*b*) and (*c*). Comparison of the stable and unstable disturbance flow patterns displayed in figures 13 and 8, respectively, does not permit identification of any characteristic element that would mark the transition

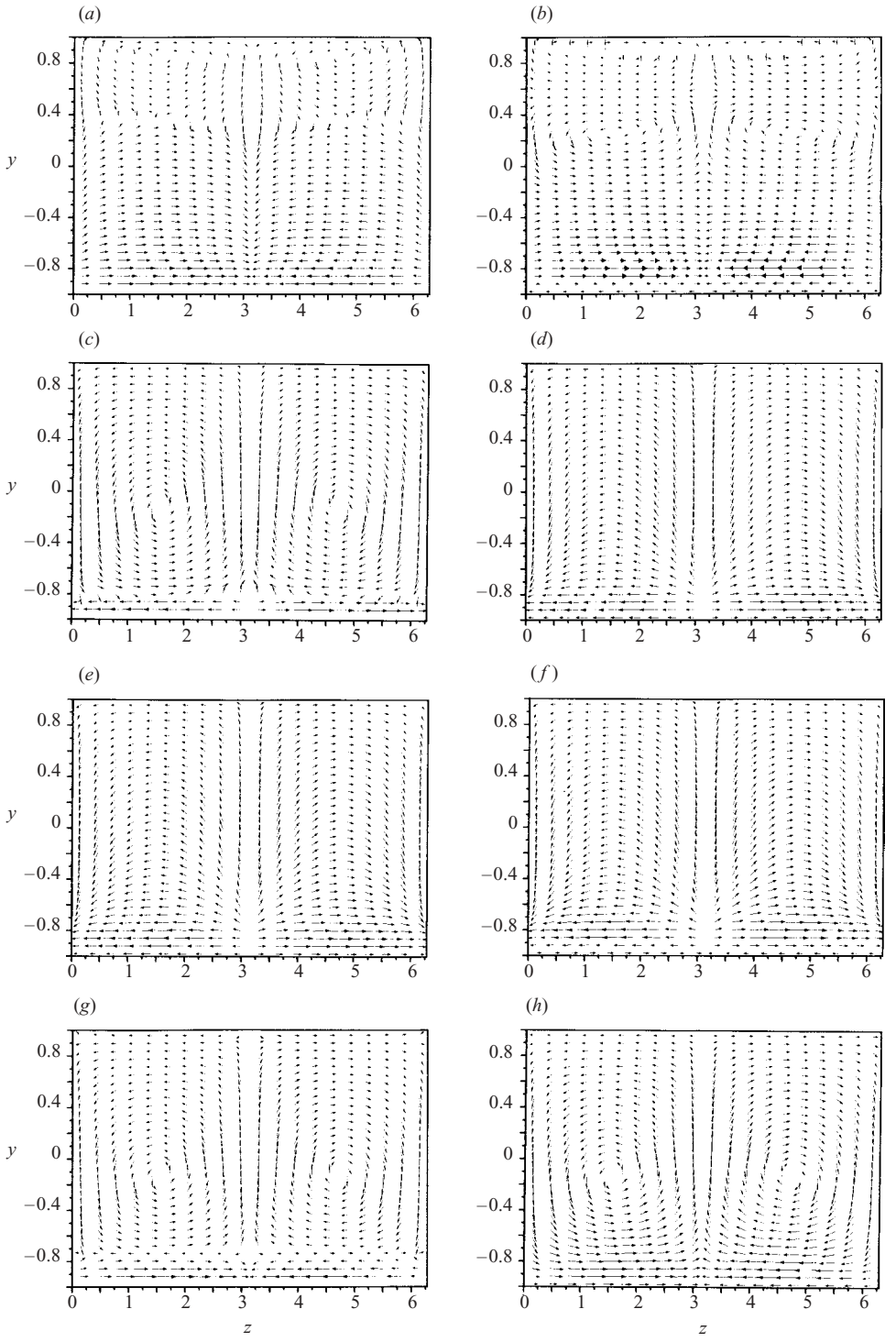

FIGURE 13. Distribution of the (y, z) component of the disturbance velocity vector for $S = 0.0001$. The remaining conditions are the same as those used in figure 8. (*a–h*) Correspond to $x = 0$, $\lambda/8$, $\lambda/4$, $3\lambda/8$, $\lambda/2$, $5\lambda/8$, $3\lambda/4$, $7\lambda/8$, respectively, where $\lambda = 2\pi/\alpha$ denotes one wavelength of wall transpiration.

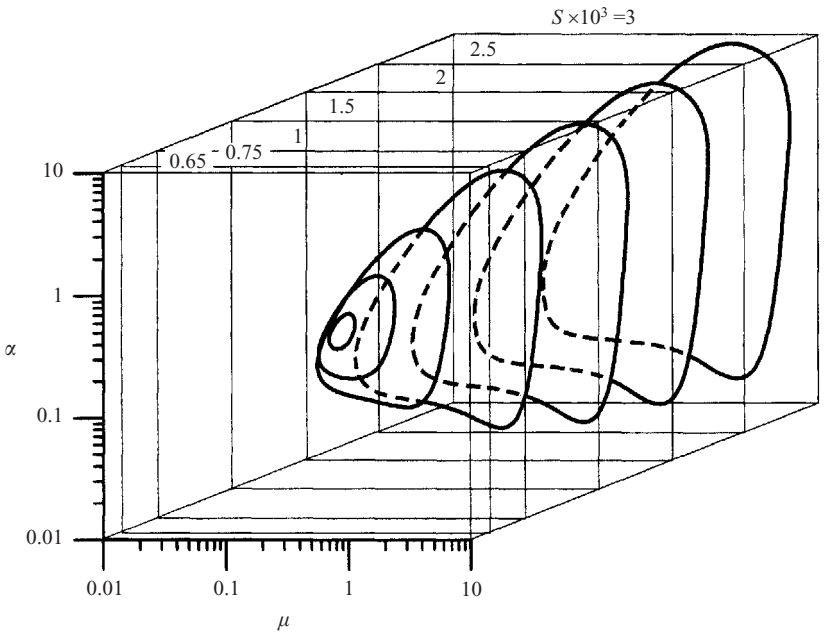

FIGURE 14. The neutral surface describing instability of Couette flow induced by wall transpiration in the form of a single Fourier mode as a function of the transpiration amplitude S, the transpiration wavenumber α and the vortex wavenumber μ for $Re = 5000$.

from stability to instability. It is the overall interplay between the destabilizing and stabilizing segments of the centrifugal force field, as well as viscous dissipation, that determine the flow response. Clearly, when the destabilizing segment of the centrifugal force field is strong enough, it is able to create vortices that can survive in most of the channel, and the flow becomes unstable.

Figure 14 displays the neutral stability surface as a function of the transpiration amplitude S, the transpiration wavenumber α and the vortex wavenumber μ for $Re = 5000$. The interior of this surface corresponds to the unstable flow conditions. It can be seen that the instability does not occur unless the amplitude S reaches a critical value defined by the tip of the neutral surface. The shape of the neutral surface shows that the range of active wavenumbers α, as well as the range of the resulting vortex wavenumbers μ, increases rapidly with an increase of S. Here we use the term 'active wavenumber' to denote transpiration wavenumber that can produce instability. Wavenumbers as high as $\alpha = 7$ and as low as $\alpha = 0.05$ can become active for $S = 0.003$. A similar surface obtained in the case of $Re = 10\,000$ is displayed in figure 15. It can be seen that destabilization as a function of S is more rapid; wavenumbers as high as $\alpha = 10$ and as low as $\alpha = 0.01$ can produce instability by $S = 0.002$.

Since it is known that the presence of vortices is a strong harbinger of transition to turbulence (Reddy *et al.* 1998; Waleffe 1997), it is interesting to determine the characteristics of the transpiration as well as the critical flow conditions that may lead to the onset of the instability. Transpiration considered here is completely defined in terms of its amplitude and wavenumber and the critical Reynolds number defining the onset of the instability has to be found for every combination of these parameters. A cut corresponding to $\alpha = \text{const}$ through the neutral surface shown in figure 14

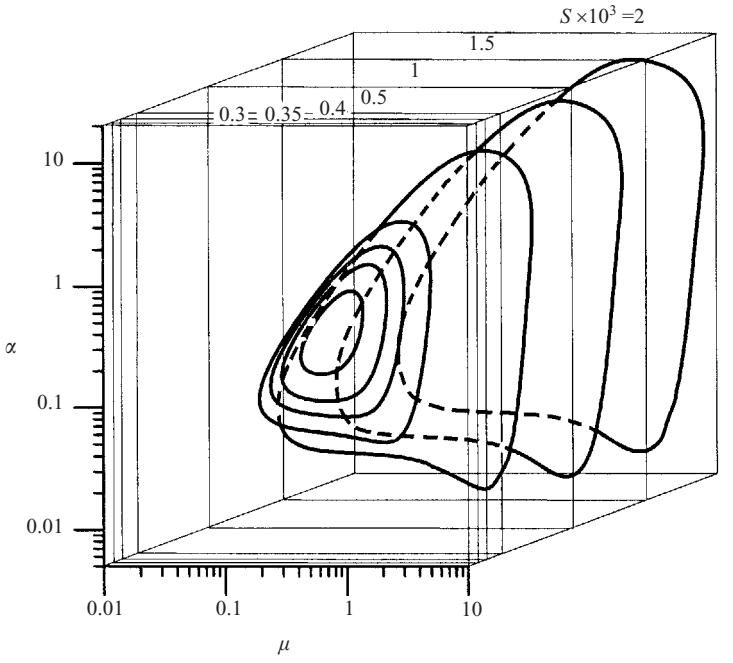

FIGURE 15. The same as figure 14 but with $Re = 10^4$.

determines the amplitude S for which $Re = 5000$ represents the critical value for this particular α. A similar cut through the neutral surface shown in figure 15 determines critical S for $Re = 10\,000$.

It is conceptually simpler to discuss the instability by fixing the form of the transpiration and studying the effect of the flow conditions, i.e. Re. Figure 16 displays the neutral surface obtained for a fixed value of $S = 0.0015$ with α, μ and Re being parameters. A strong role of Re in the destabilization process is clearly visible. A cut corresponding to $\alpha = \text{const}$ determines the critical Re for this particular α and S. It is convenient for presentation of the results to introduce the global critical Reynolds number $Re_{g,cr}$ that defines the critical conditions for the given amplitude of the transpiration regardless of its wavenumber. Such global critical conditions, which include the critical transpiration wavenumber $\alpha_{g,cr}$ and the critical vortex wavenumber $\mu_{g,cr}$, correspond to the tip of the neutral surface shown in figure 16. Variations of the global critical conditions as a function of S are shown in figure 17. The area below the critical curve defines the range of the transpiration amplitudes and the flow Reynolds numbers where flow instability never occurs regardless of the transpiration wavenumber. Above this curve instability may occur, but only for a well-defined range of α.

Experimental results on Couette flow do not provide accurate information about the level of disturbances present. One may view flow modifications induced by wall transpiration as representing as a certain class of disturbances. Since nonlinear effects typically become active at about 1% disturbance level (i.e. $S = 0.05$), data presented in figure 17 estimate the critical Reynolds number to be about $Re_{g,cr} \sim 800$, which compares well with the experimental value of $Re = 600$–800 required for the natural transition.

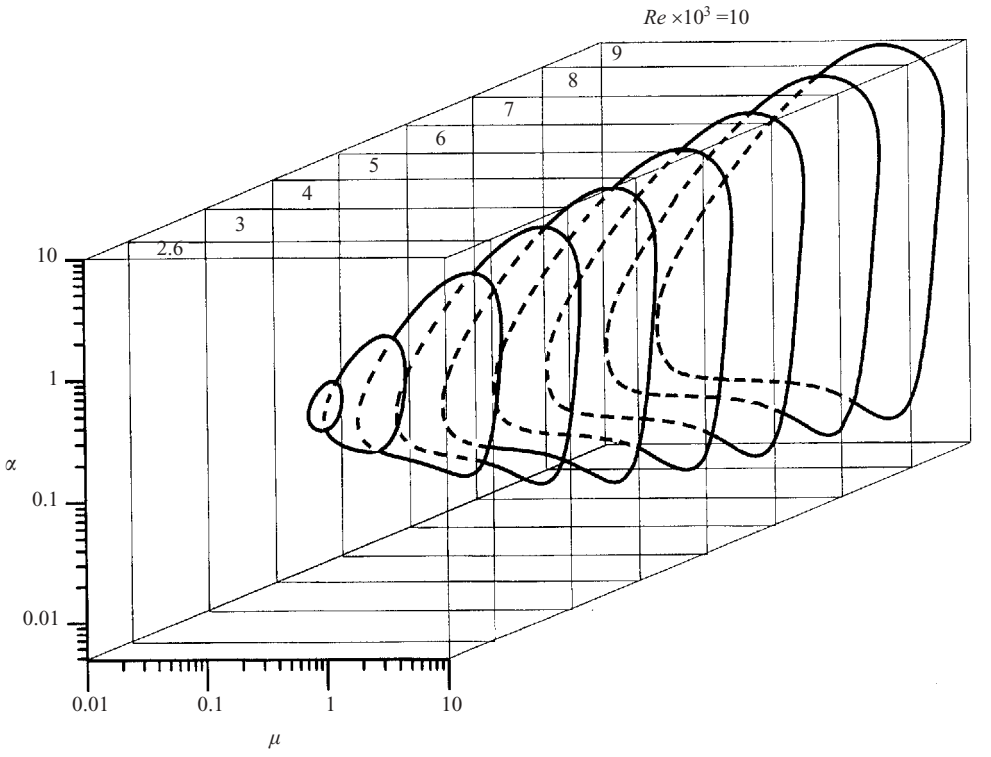

FIGURE 16. The neutral surface describing instability of Couette flow induced by the wall transpiration as a function of the flow Reynolds number Re, the transpiration wavenumber α and the vortex wavenumber μ. The transpiration has the form of a single Fourier mode with the amplitude $S = 0.0015$. The tip of this surface defines the global critical conditions $(Re_{g,cr}, \alpha_{g,cr}, \mu_{g,cr})$.

The critical curve $Re_{g,cr}(S)$ defines the threshold for the base flow modifications required for the onset of the instability. The available results show that this threshold decreases as $Re^{-1.15}$ for large Re. Since these results were obtained with the transpiration in the form of a single Fourier harmonic, different thresholds may exist for other forms of transpiration. It should be stressed that instability will not occur above the threshold unless the flow modifications have a specific form defined by the critical wavenumber α.

Figure 17 also displays the critical curve in terms of the transpiration Reynolds number $Re_t = SRe$ rather than the transpiration amplitude S. The threshold value of Re_t required for the instability varies as $Re^{-0.15}$ for large values of Re.

The form of the critical curve suggests that there exists an absolute minimum for the global critical Reynolds number below which the transpiration, regardless of its amplitude, cannot destabilize the flow. It can be seen from magnification of the lower end of the critical curve, shown in a linear scale in figure 18, that the instability does occur if $Re < 84$. This defines the global threshold.

4.2. *Instability in the case of low Reynolds numbers*

The fact that the instability associated with the wall transpiration may occur for Re significantly smaller then the transition Re observed in the absence of transpiration (Tillmark & Alfredsson 1992; Daviaud *et al.* 1992) justifies a closer look at the

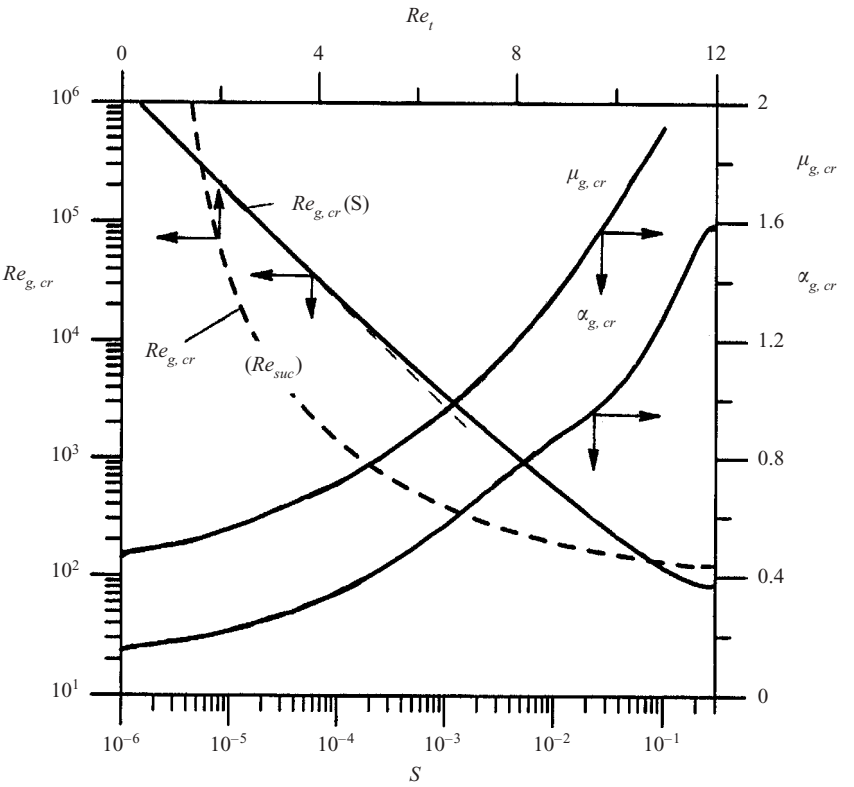

FIGURE 17. Variations of the global critical stability conditions $(Re_{g,cr}, \alpha_{g,cr}, \mu_{g,cr})$ as a function of the amplitude S of the transpiration. Asymptote for $Re_{g,cr}$ at large values of Re is represented with a thin dashed line. Thick dashed line gives variations of $Re_{g,cr}$ as a function of the transpiration Reynolds number Re_t. An enlargement of the critical curve for low values of Re is displayed in figure 18.

disturbance motion at low Re near the onset. All results presented in this section have been obtained with $Re = 182$. The reader may recall that the base flow modifications are strongly nonlinear for these flow conditions and that an accurate representation of the disturbance motion requires a significant number of Fourier modes, as illustrated by the results presented in tables 3 and 4.

We begin the discussion with a description of the base flow. Streamline of this flow as well as streamlines curvature and flow circulation are illustrated in figure 19 for $\alpha = 1.1$, $S = 0.05$. They are qualitatively similar to the flow at $Re = 5000$ shown in figure 4, with all characteristic features being more pronounced. Bubbles containing fluid transferred through the wall extend well into the interior of the channel, the curvature of the streamlines is bigger, the gradient of the circulation is smaller and the potentially unstable zone is more constrained. The last two facts combined with the presence of strong viscous damping suggest the need for a strong transpiration in order to produce the instability.

The neutral surface as a function of α, μ and Re for fixed $S = 0.05$ is shown in figure 20. It can be seen that both the range of active transpiration wavenumbers α and the range of the resulting vortex wavenumbers μ are very limited; the 'window of opportunity' for creation of this instability is severely constrained.

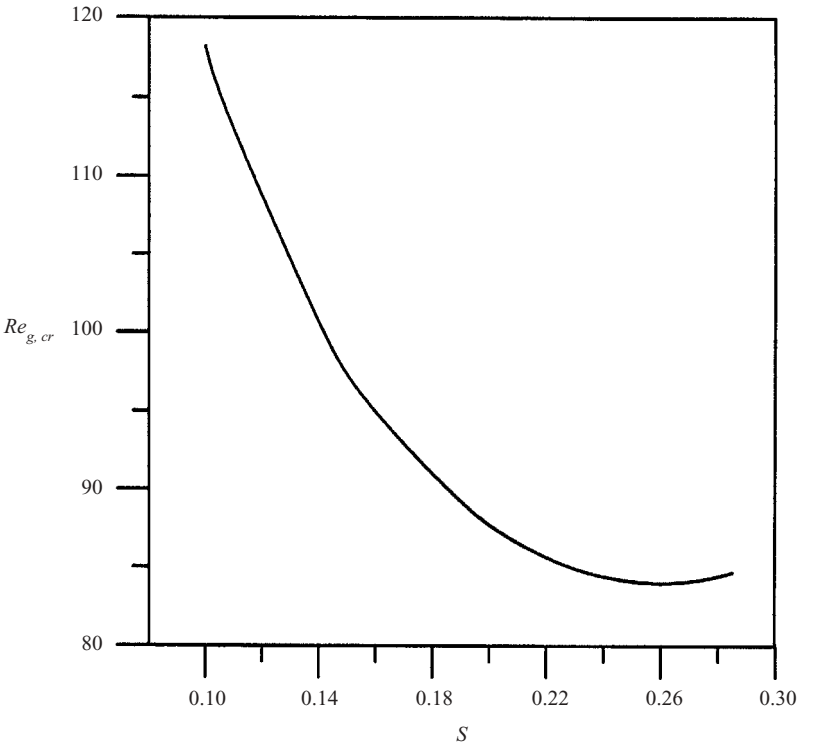

FIGURE 18. Global critical stability curve $Re_{g,cr}(S)$ for low values of the flow Reynolds number Re.

Figure 21 displays the form of the first three eigenfunctions associated with the vortices for $\mu = 1.75, \alpha = 1.1, S = 0.05$ and $Re = 182$. The dominant character of $g_u^{(0)}$ is retained but the role of the higher modes is more pronounced. The form of the velocity amplitude function $\boldsymbol{h}_3(x, y)$ (see (3.5)) displayed in figure 22 is quite complex, with a large change in h_u suggesting strong streamwise vortex modulation effects. This expectation is confirmed by plots of transverse velocity vector in the (y, z)-plane displayed in figure 23. We start with one pair of counter-rotating vortices at $x = 0$ (figure 23*a*). A second, fairly large, layer of vortices can be seen forming at the bottom of the channel at $x = \lambda/8$ (figure 23*b*). This second layer is well-developed at $x = \lambda/4$ (figure 23*c*) and still exists at $x = 3\lambda/8$ (figure 23*d*) although the beginning of the formation of the jet-like structure at the lower wall can be identified. There is no sign of vortex structure at $x = \lambda/2$ and at $x = 5\lambda/8$ (figure 23*e* and figure 23*f*). Vortices re-emerge at $x = 3\lambda/4$ (figure 23*g*) and are well-established at $x = 7\lambda/8$ (figure 23*h*). The effects of streamwise vortex modulation, which give the appearance of the existence of sinks and sources in figure 23*e* and figure 23*f*, and lead to elimination and re-creation of vortices between figures 23(*d*) and 23(*g*), as well as creation and elimination of the second layer of vortices between figures 23(*a*) and 23(*e*), are clearly visible.

Figure 24 illustrates variations of the vortex amplification rate as a function of the transpiration amplitude S. Squire's mode is recovered in the limit of $S \to 0$, as expected. The structure of the disturbance velocity field at very small values of S (not shown) is qualitatively very similar to the structure discussed in the previous section for $Re = 5000$ (figure 11), with the higher Fourier modes being relatively stronger.

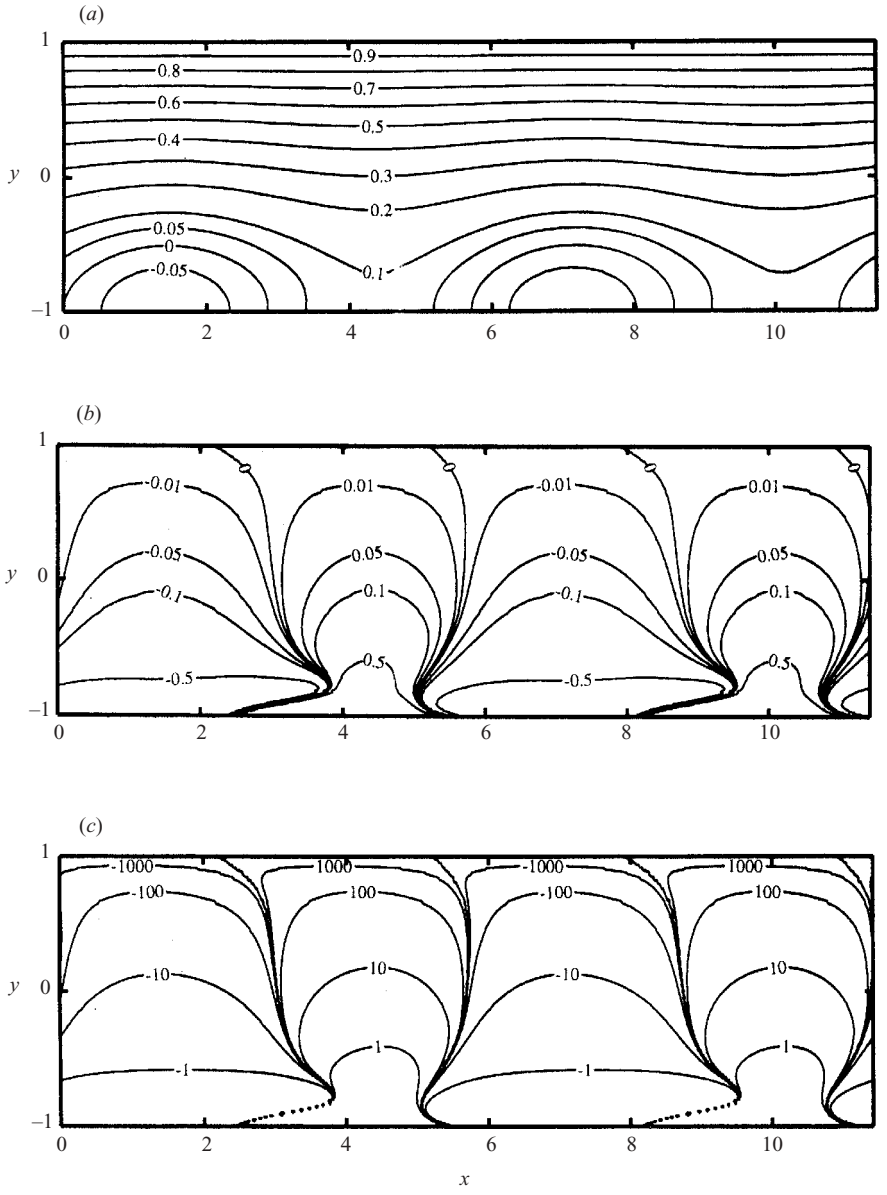

FIGURE 19. Form of base flow resulting from the presence of transpiration with wavenumber $\alpha = 1.1$ and amplitude $S = 0.05$ for $Re = 182$ and $x \in (0, 4\pi/\alpha)$. (*a–d*) Streamline pattern, streamline curvature, (4.1), and circulation, (4.2), respectively.

5. Summary

Linear stability of plane Couette flow modified by transpiration applied at the lower wall has been considered. While the problem formulation considers arbitrary distribution of transpiration, the explicit results are given in the case of transpiration in the form of a single Fourier harmonic described uniquely in terms of the wavenumber α and the amplitude S.

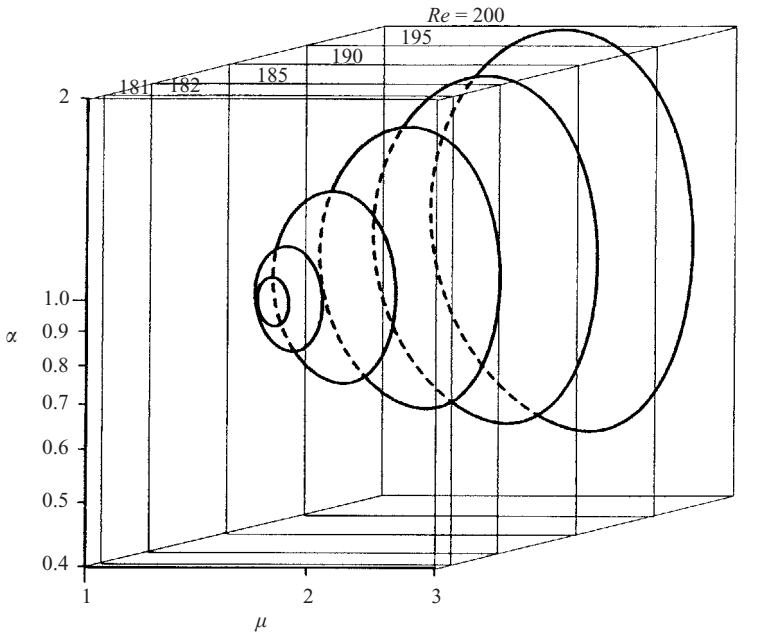

FIGURE 20. The neutral surface describing instability of Couette flow induced by wall transpiration as a function of the flow Reynolds number Re, the transpiration wavenumber α and the vortex wavenumber μ. The transpiration has the form of a single Fourier mode with the amplitude $S = 0.05$.

Results of a stability analysis show that the introduction of transpiration can destabilize the flow at finite Reynolds numbers. The instability manifests itself through the generation of streamwise-vortex-like structures and is attributed to centrifugal effects. The presence of transpiration produces bubbles of fluid transferred through the wall that act as obstacles for the fluid flowing through the channel and force this fluid to change direction. The resulting streamline curvature gives rise to centrifugal forces that drive the instability. The resulting unstable motion can be described as streamwise vortices modulated by streamwise variations of transpiration, resulting in a complex topology of the disturbance velocity field. No other disturbances have been considered and thus all conclusions apply only to streamwise vortices. In particular, the possible occurrence of travelling wave instability has not been considered.

The instability occurs only if the flow Reynolds number Re and the transpiration amplitude S are large enough. If these conditions are met, the instability occurs only for a certain finite range of the transpiration wavenumber α and gives rise to a certain finite range of streamwise vortex wavenumbers μ. Since a description of the neutral stability surface requires four-dimensional space, one has to look at various cross-sections of this surface. Results illustrating the magnitude of S required for the onset of the instability, the range of 'active' α and the range of resulting μ for several values of Re have been presented. The strength of the instability, as measured by the amplification rate, increases with the increase of the transpiration amplitude S and the flow Reynolds number Re. The range of the 'active' wavenumbers α and the range of the resulting vortex wavenumbers μ also increase with the increase of S and Re.

The critical flow conditions expressed in terms of the critical Reynolds number leading to the onset of the instability can be found for each combination of the

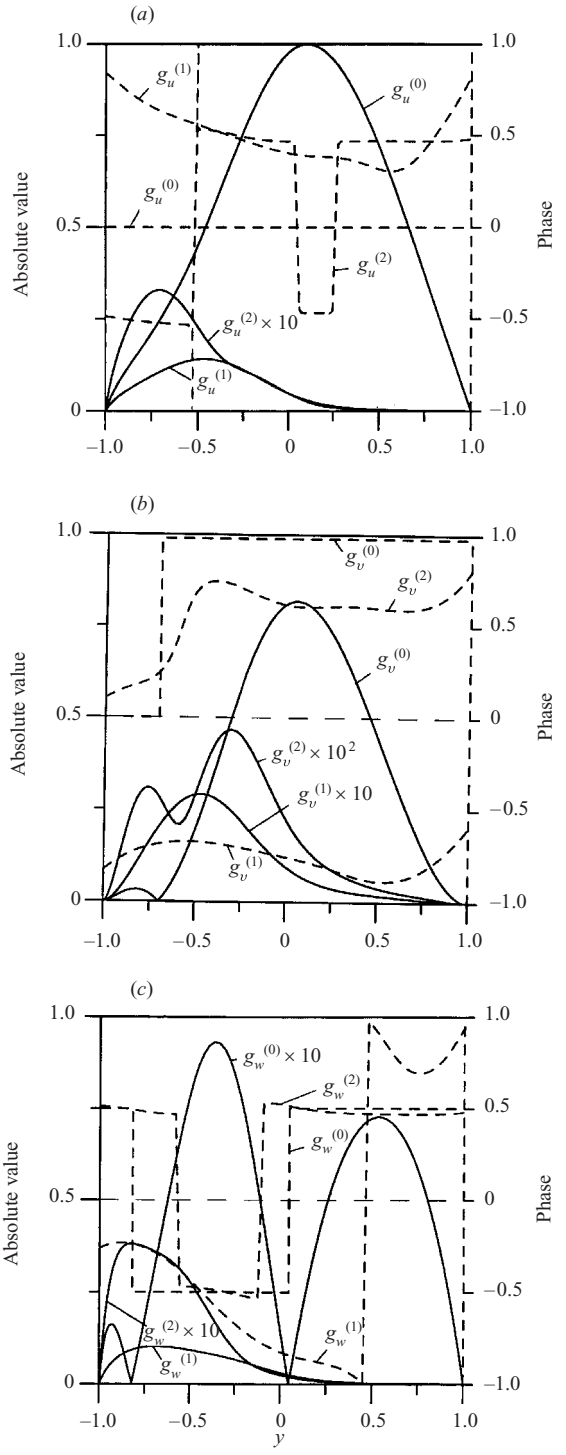

FIGURE 21. Eigenfunctions $g_u^{(m)}, g_v^{(m)}, g_w^{(m)}, m = 0, 1, 2$, describing a vortex with wavenumber $\mu = 1.75$ induced by wall transpiration with wavenumber $\alpha = 1.1$ and amplitude $S = 0.05$ for the flow Reynolds number $Re = 182$ and normalized with condition $\max(g_u^{(0)}) = 1$. (*a–c*) Functions $g_u^{(m)}, g_v^{(m)}, g_w^{(m)}$, respectively.

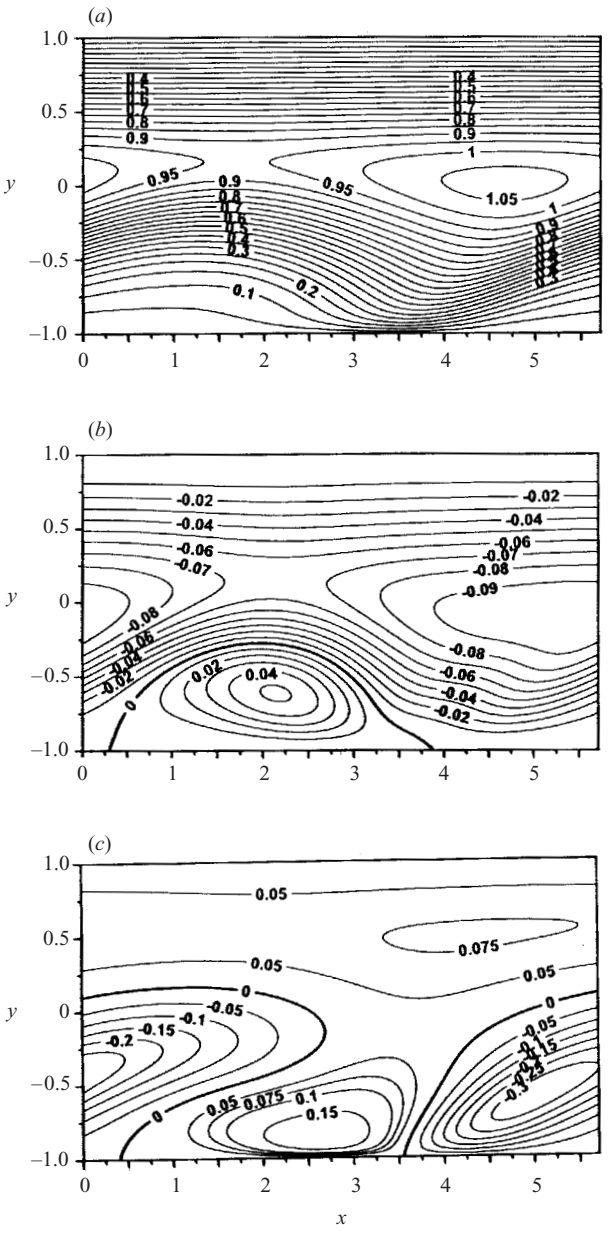

FIGURE 22. Velocity amplitude function $\boldsymbol{h}_3(x, y) = [h_u(x, y), h_v(x, y), \mathrm{i}\hat{h}_w(x, y)]$ (see (3.5)) for $Re = 182$, $\alpha = 1.1$, $\mu = 1.75$, $S = 0.05$ normalized with condition $\max(g_u^{(0)}) = 1$. (*a–c*) Functions h_u, h_v, $\hat{h}_w$, respectively.

transpiration amplitude S and the transpiration wavenumber α. The global critical conditions expressed in terms of the global critical Reynolds number leading to the onset of the instability for the given transpiration amplitude S regardless of its wavenumber α have been determined. These conditions determine the transpiration threshold (minimum transpiration amplitude) required for the onset. This threshold varies with flow Reynolds number as $\sim Re^{-1.15}$ for large Re. The existence of a global

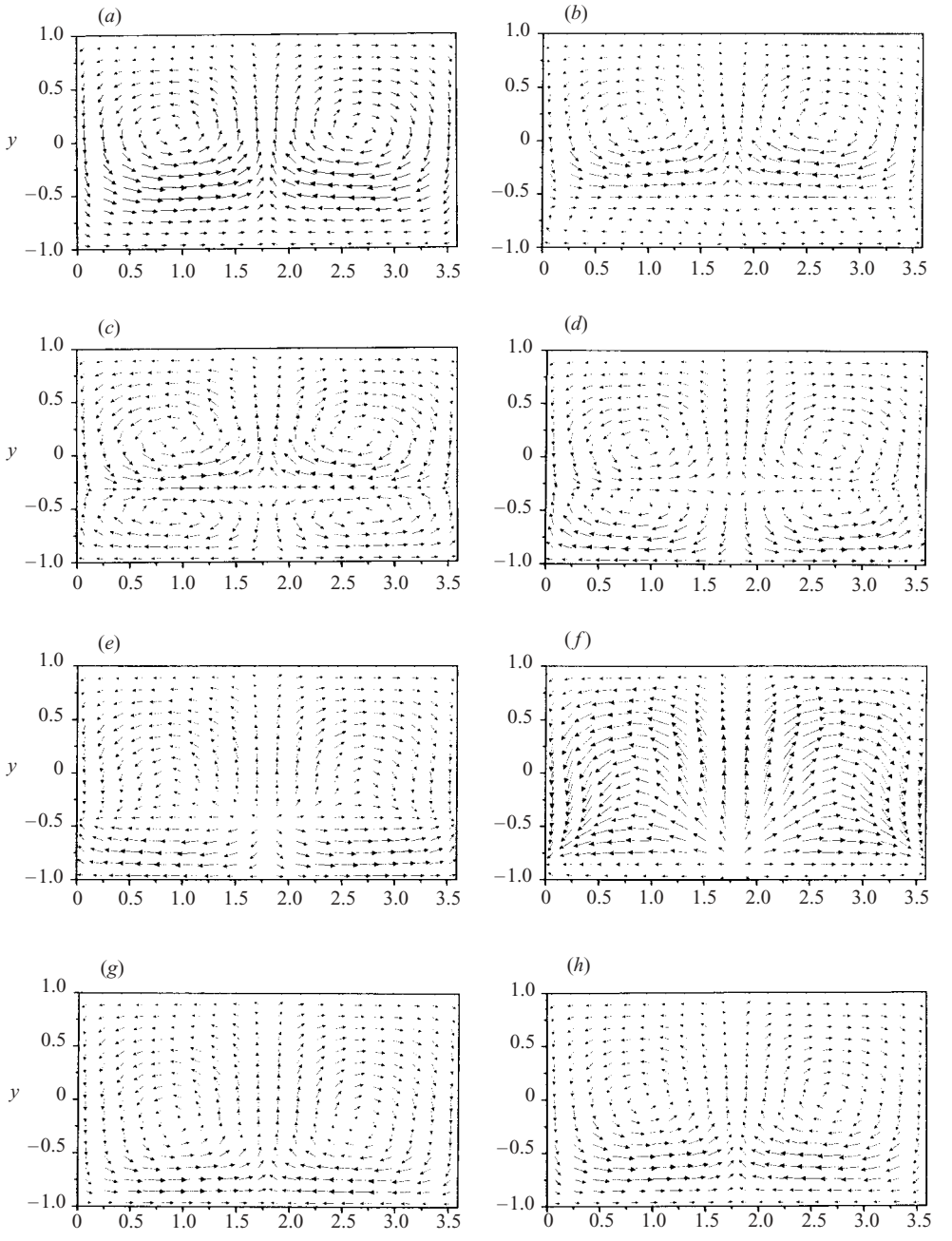

FIGURE 23. Distribution of the (y, z) component of the disturbance velocity vector for $z \in (0, 2\pi/\mu)$, $\mu = 1.75$, $\alpha = 1.1$, $Re = 182$, $S = 0.05$. The disturbance velocity vector is normalized with condition $\max(g_u^{(0)}) = 1$. (*a–h*) Correspond to $x = 0, \lambda/8, \lambda/4, 3\lambda/8, \lambda/2, 5\lambda/8, 3\lambda/4, 7\lambda/8$, respectively, where $\lambda = 2\pi/\alpha$ denotes one wavelength of wall transpiration.

threshold, where the instability does not occur regardless of the magnitude of the transpiration, has been demonstrated. The global threshold occurs at $Re \approx 84$.

Flow modifications associated with wall transpiration can be viewed as a class of natural flow disturbances. The global critical Reynolds number corresponding to

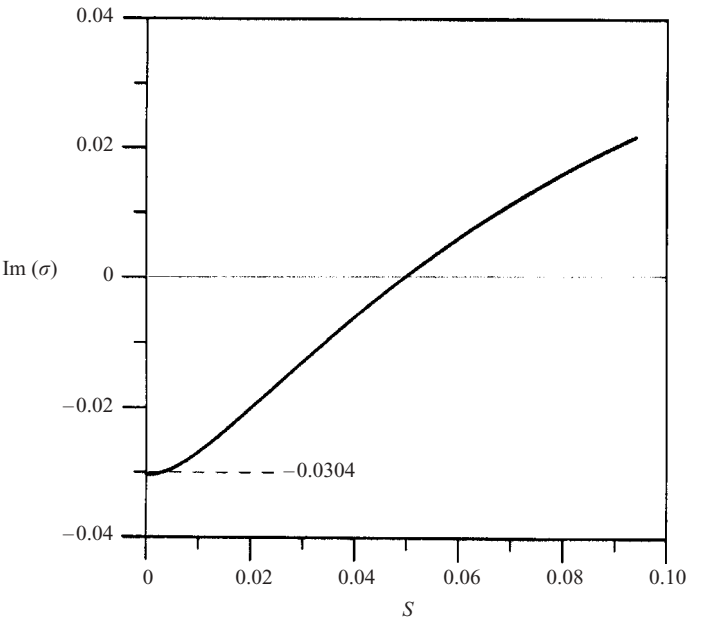

FIGURE 24. Variations of the amplification rate Im(σ) of streamwise vortices with wavenumber $\mu = 1.75$ induced by wall transpiration with wavenumber $\alpha = 1.1$ for $Re = 182$ as a function of the transpiration amplitude S.

a 1% level of such disturbances corresponds well to the experimentally determined natural transition Reynolds number.

This work has been carried out with support of NSERC of Canada, de Havilland and Canadair. Drs J. Szumbarski and S. Krol have written one of the codes used in the computations. The author would like to thank Dr S. Krol and M. Floryan for assistance in carrying out computations.

Appendix A

The solution of problem (2.17) can be expressed in the limit $\alpha \to 0$, following the method described by Floryan & Dallmann (1990), in the form

$$\Phi_1 = S\left\{\alpha^{-1}\tfrac{1}{4}\mathrm{i}(y^3 - 3y + 2) + \frac{Re}{480}[-y^6 + 3y^2 - 2 + 3(-y^5 + 2y^3 - y)] + O(\alpha)\right\}.$$

When $\alpha \to \infty$, the solution takes the form

$$\Phi_1 = S\mathrm{e}^{-\xi}\left\{\alpha^{-1}\mathrm{i}(1+\xi) + \alpha^{-3}Re\left[\tfrac{1}{8}\xi^2 + \tfrac{1}{24}\xi^3\right] + 0(\alpha^{-4})\right\}$$

where $\xi = \alpha(y+1)$. When $Re = 0$, the solution has the form

$$\Phi_1 = A_1\sinh(\alpha y) + A_2\cosh(\alpha y) + A_3\, y\sinh(\alpha y) + A_4\, y\cosh(\alpha y)$$

where the constants A_1, A_2, A_3, A_4 have the form

$$A_1 = \frac{\mathrm{i}S}{2}[-\alpha^{-1}\sinh^{-1}(\alpha) + \cosh^2(\alpha)\sinh^{-1}(\alpha)(\alpha - \sinh(\alpha)\cosh(\alpha))^{-1}],$$

$$A_2 = \frac{\mathrm{i}S}{2}[\alpha^{-1}\cosh^{-1}(\alpha) + \sinh^2(\alpha)\cosh^{-1}(\alpha)(\alpha + \sinh(\alpha)\cosh(\alpha))^{-1}],$$

$$A_3 = -\frac{\mathrm{i}S}{2}\sinh(\alpha)(\alpha + \sinh(\alpha)\cosh(\alpha))^{-1}, \quad A_4 = -\frac{\mathrm{i}S}{2}\cosh(\alpha)(\alpha - \sinh(\alpha)\cosh(\alpha))^{-1}.$$

The solution in the inviscid limit has the form

$$\Phi_1 = \frac{\mathrm{i}S}{2\alpha}\left[\frac{\cosh(\alpha y)}{\cosh(\alpha)} - \frac{\sinh(\alpha y)}{\sinh(\alpha)}\right].$$

The solution for large but finite Re can be expressed in terms of Airy's functions using techniques described by Drazin & Reid (1981).

Appendix B

The operators is equations (3.8) and (3.9) are given by

$$S^{(m)} = \mathrm{D}^2 - k_m^2 - \mathrm{i}Re(t_m u_0 - \sigma), \tag{B 1}$$

$$T^{(m)} = \left(\mathrm{D}^2 - k_m^2\right)^2 - \mathrm{i}Re\left[(t_m u_0 - \sigma)\left(\mathrm{D}^2 - k_m^2\right)\right], \tag{B 2}$$

$$C = Re\mu\mathrm{D}u_0, \tag{B 3}$$

$$W_u^{(m,n)} = \mu\left(\mathrm{i}f_v^{(n)}\mathrm{D} - t_m f_u^{(n)}\right), \tag{B 4}$$

$$W_v^{(m,n)} = \mathrm{i}\mu\mathrm{D}f_u^{(n)}, \tag{B 5}$$

$$W_w^{(m,n)} = t_m\left(t_{m-n}f_u^{(n)} - \mathrm{i}f_v^{(n)}\mathrm{D}\right), \tag{B 6}$$

$$B_u^{(m,n)} = -t_m^2\mathrm{D}f_u^{(n)} + \mathrm{i}n\alpha k_m^2 f_v^{(n)} - t_m^2 f_u^{(n)}\mathrm{D} + \mathrm{i}t_m\mathrm{D}f_u^{(n)}\mathrm{D} + \mathrm{i}t_m f_v^{(n)}\mathrm{D}^2, \tag{B 7}$$

$$B_v^{(m,n)} = \mathrm{i}k_m^2 t_{m-n}f_u^{(n)} + k_m^2\mathrm{D}f_v^{(n)} + k_m^2 f_v^{(n)}\mathrm{D} + \mathrm{i}t_m\mathrm{D}^2 f_u^{(n)} + \mathrm{i}t_m\mathrm{D}f_u^{(n)}\mathrm{D}, \tag{B 8}$$

$$B_w^{(m,n)} = \mu\left(-t_{m-2n}f_u^{(n)}\mathrm{D} - t_{m-n}\mathrm{D}f_u^{(n)} + \mathrm{i}f_v^{(n)}\mathrm{D}^2\right), \tag{B 9}$$

$$E_v^{(m,n)} = \mu\left(-\mathrm{D}f_u^{(n)} + \mathrm{i}n\alpha k_{m-n}^{-2}f_v^{(n)}\mathrm{D}^2\right), \tag{B 10}$$

$$E_\theta^{(m,n)} = \mathrm{i}t_m f_u^{(n)} + \left(1 + n\alpha t_{m-n}k_{m-n}^{-2}\right)f_v^{(n)}\mathrm{D}, \tag{B 11}$$

$$\begin{aligned} H_v^{(m,n)} = {} & \mathrm{i}n\alpha k_{m-n}^{-2}(\mu^2 - t_m t_{m-n})\mathrm{D}f_u^{(n)}\mathrm{D} + k_m^2 k_{m-n}^{-2}(\mu^2 + t_{m-n}t_{m-2n})f_v^{(n)}\mathrm{D} \\ & + \mathrm{i}k_{m-n}^{-2}\left(-k_{m-n}^2 t_m + 2n\alpha\mu\right)f_u^{(n)}\mathrm{D}^2 + k_{m-n}^{-2}\left(n\alpha t_m - k_m^2\right)f_v^{(n)}\mathrm{D}^3 \\ & + \mathrm{i}k_m^2 t_{m-2n}f_u^{(n)} + \mathrm{i}t_m\mathrm{D}^2 f_u^{(n)}, \end{aligned} \tag{B 12}$$

$$\begin{aligned} H_\theta^{(m,n)} = {} & n\alpha\mu\left(2t_{m-n}k_{m-n}^{-2}f_u^{(n)}\mathrm{D} + k_{m-n}^{-2}(t_m + t_{m-n})\mathrm{D}f_u^{(n)} - \mathrm{i}k_m^2 k_{m-n}^{-2}f_v^{(n)}\right. \\ & \left. - \mathrm{i}k_{m-n}^{-2}f_v^{(n)}\mathrm{D}^2\right), \end{aligned} \tag{B 13}$$

where $k_m^2 = t_m^2 + \mu^2$.

REFERENCES

Aydin, M. & Leutheusser, H. J. 1979 Novel experimental facility for study of plane Couette flow. *Rev. Sci. Instrum.* **50**, 1362–1366.

Barkley, D. & Tuckerman, L. S. 1999 Stability analysis of perturbed plane Couette flow. *Phys. Fluids* **11**, 1187–1195.

Benmalek, A. & Saric, W. S. 1994 Effects of curvature variations on the nonlinear evolution of Görtler vortices. *Phys. Fluids* **6**, 3353–3367.

Bottaro, A., Corbett, P. & Luchini, L. 2003 The effect of base-flow variation on flow stability. *J. Fluid. Mech.* **476**, 293–302.

Bottin, S. & Chaté, H. 1998 Statistical analysis of the transition to turbulence in plane Couette flow. *Eur. Phys. J.* B **6**, 143–155.

Bottin, S., Dauchot, O. & Daviaud, F. 1998*a* Experimental evidence of streamwise vortices as finite amplitude solutions in transitional plane Couette flow. *Phys. Fluids* **10**, 2597–2607.

Bottin, S., Manneville, P., Daviaud, F. & Dauchot, O. 1998*b* Discontinuous transition to spatio-temporal intermittency in plane Couette flow. *Europhys. Lett.* **43**, 171–176.

Butler, K. M. & Farrell, B. F. 1992 Three-dimensional optimal perturbations in viscous shear flow. *Phys. Fluids* A **4**, 1637–1650.

Canuto, C., Hussaini, M. Y., Quarteroni, A. & Zang, T. A. 1988 *Spectral Methods in Fluid Dynamics*. Springer.

Chapman, S. J. 2002 Sub-critical transition in channel flow. *J. Fluid Mech.* **451**, 35–97.

Cherhabili, A. & Ehrenstein, U. 1995 Spatially localized two-dimensional finite-amplitude states in plane Couette flow. *Eur. J. Mech.* B/*Fluids* **14**, 677–696.

Cherhabili, A. & Ehrenstein, U. 1997 Finite-amplitude equilibrium states in plane Couette flow. *J. Fluid Mech.* **342**, 159–177.

Clever, R. M. & Busse, F. H. 1992 Three-dimensional convection in a horizontal fluid layer subjected to a constant shear. *J. Fluid Mech.* **234**, 511–527.

Clever, R. M. & Busse, F. H. 1997 Tertiary and quaternary solutions for plane Couette flow. *J. Fluid Mech.* **344**, 137–153.

Coddington, E. A. & Levinson, N. 1965 *Theory of Ordinary Differential Equations*. McGraw-Hill.

Craik, A. D. D. 1982 Wave-induced longitudinal-vortex instability in shear flows. *J. Fluid Mech.* **125**, 37–82.

Craik, A. D. D. & Leibovich, S. 1976 A rational model for Langmuir circulation. *J. Fluid Mech.* **73**, 401–426.

Dauchot, O. & Daviaud, F. 1995*a* Finite-amplitude perturbation and spot growth mechanism in plane Couette flow. *Phys. Fluids* **7**, 335–343.

Dauchot, O. & Daviaud, F. 1995*b* Streamwise vortices in plane Couette flow. *Phys. Fluids* **7**, 901–903.

Daviaud, F., Hegseth, J. & Bergé, P. 1992 Subcritical transition to turbulence in plane Couette flow. *Phys. Rev. Lett.* **69**, 2511–2514.

Dean, W. 1928 Fluid motion in a curved channel. *Proc. R. Soc. Lond.* A **121**, 402–420.

Drazin, P. G. & Reid, W. H. 1981 *Hydrodynamic Stability*. Cambridge University Press.

Dubrulle, B. & Zahn, J. P. 1991 Nonlinear instability of viscous plane Couette flow. Part 1. Analytical approach to necessary condition. *J. Fluid Mech.* **231**, 561–573.

Floryan, J. M. 1986 Görtler instability of boundary layers over concave and convex walls. *Phys. Fluids* **29**, 2380–2387.

Floryan, J. M. 1997 Stability of wall-bounded shear layers in the presence of simulated distributed roughness. *J. Fluid Mech.* **335**, 29–55.

Floryan, J. M. 2002 Centrifugal instability of Couette flow over a wavy wall. *Phys. Fluids* **14**, 312–322.

Floryan, J. M. & Dallmann, U. 1990 Flow over a leading edge with distributed roughness. *J. Fluid Mech.* **216**, 629–656.

Floryan, J. M., Yamamoto, K. & Murase, T. 1992 Laminar-turbulent transition process in the presence of simulated wall roughness. *Can. Aeronaut. Space Inst. J.* **38**, 173–182.

Glezer, A. & Amitay, M. 2002 Synthetic jets. *Annu. Rev. Fluid Mech.* **34**, 503–529.

Görtler, H. 1941 Instabilität laminarer Grenzschichten an konkaven Wänden gegenüber gewissen dreidimensionalen Störungen. *Z. Angew. Math. Mech.* **21**, 250–252.

Görtler, H. & Witting, H. 1958 Theorie der sekundären Instabilität der laminaren Grenzschichten. *Proc. Symp. on Boundary Layer Research, IUTAM*, pp. 110–126 Springer.

Hamilton, J. M., Kim, J. & Waleffe, F. 1995 Regeneration mechanism of near-wall turbulence structures. *J. Fluid Mech.* **287**, 317–348.

Kreiss, G., Lundbladh, A. & Henningson, D. S. 1994 Bounds for threshold amplitudes in sub-critical shear flow. *J. Fluid Mech.* **270**, 175–198.

Leibovich, S. 1977 Convective instability of stably stratified water in the ocean. *J. Fluid Mech.* **82**, 561–585.

Leibovich, S. 1983 The form and dynamics of Langmuir circulation. *Annu. Rev. Fluid Mech.* **15**, 391–427.

Lerner, J. & Knobloch, E. 1988 The long-wave instability of a defect in a uniform parallel shear. *J. Fluid Mech.* **189**, 117–134.

Leutheusser, H. J. & Chu, V. H. 1971 Experiments on plane Couette flow. *J. Hydraul. Div. ASCE* **97**, 1269–1284.

Lundbladh, A. & Johansson, A. V. 1991 Direct simulation of turbulent spots in plane Couette flow. *J. Fluid Mech.* **229**, 499–516.

Malerud, S., Måløy, K. J. & Goldburg, W. I. 1995 Measurements of turbulent velocity fluctuations in a planar Couette cell. *Phys. Fluids* **7**, 1949–1955.

Morkovin, M. V. 1990 On the roughness-induced transition: facts, views and speculations. In *Instability and Transition* (ed. M. Y. Hussaini & R. G. Voigt), vol. 1, pp. 281–295. ICASE/ NASA LARC Series, Springer.

Nagata, M. 1990 Three-dimensional finite-amplitude solutions in plane Couette flow: bifurcation from infinity. *J. Fluid Mech.* **217**, 519–527.

Orszag, S. A. & Patera, A. T. 1983 Secondary instability of wall-bounded flows. *J. Fluid Mech.* **128**, 347–385.

Phillips, W. R. C. 1998 On the nonlinear instability of strong wavy shear to longitudinal vortices. In *Nonlinear Instability, Chaos and Turbulence.* (ed. L. Debnath & D. N. Riahi), pp. 251–273. Comp. Mech. Publications.

Phillips, W. R. C. & Wu, Z. 1994 On the instability of wave-catalysed longitudinal vortices in strong shear. *J. Fluid Mech.* **272**, 235–254.

Phillips, W. R. C., Wu, Z. & Lumley, J. L. 1996 On the formation of longitudinal vortices in a turbulent boundary layer over wavy terrain. *J. Fluid Mech.* **326**, 321–341.

Rayleigh, Lord 1916 On the dynamics of the revolving fluids. *Proc. R. Soc. Lond.* A **93**, 148–154.

Reddy, S. C., Schmid, P. J., Bagget, J. S. & Henningson, D. S. 1998 On stability of streamwise streaks and transition thresholds in plane channel flows. *J. Fluid Mech.* **365**, 269–303.

Romanov, V. A. 1972 Stability of plane-parallel Couette flow. *Funct. Anal. Applics.* **7**, 137–146.

Saric, W. S. & Benmalek, A. 1991 Görtler vortices with periodic curvature. *Boundary Layer and Transition to Turbulence. ASME* FED-vol. 114.

Saric, W. S., Reed, H. L. & Kerschen, E. J. 2002 Boundary-layer receptivity to freestream disturbances. *Annu. Rev. Fluid Mech.* **34**, 291–319.

Saric, W. S., Reed, H. L. & White, E. B. 2003 Stability and transition of three-dimensional boundary layers. *Annu. Rev. Fluid Mech.* **35**, 413–440.

Schmid, P. J. & Henningson, D. S. 2001 *Stability and Transition in Shear Flows.* Applied Mathematical Sciences, vol. 142, Springer.

Taylor, G. 1923 Stability of viscous liquid contained between two rotating cylinders. *Phil. Trans. R. Soc.* A **223**, 289–293.

Tillmark, N. & Alfredsson, P. H. 1992 Experiments on transition in plane Couette flow. *J. Fluid Mech.* **235**, 89–102.

Tokuda, M. 1972 Taylor-Görtler vortices expected in the air flow on sea surface waves. *J. Oceanogr. Soc. Japan* **28**, 242–253.

Trefethen, L. N., Trefethen, A. E., Reddy, S. C. & Driscoll, T. A. 1993 Hydrodynamic stability without eigenvalues. *Science* **261**, 578–584.

Waleffe, F. 1997 On a self-sustaining process in shear flows. *Phys. Fluids* **9**, 883–900.